Inorganic Chemistry

pubs.acs.org/IC

Article

MLCT Excited-State Behavior of Trinuclear Ruthenium(II) 2,2′-Bipyridine Complexes

Simon Cerfontaine, Ludovic Troian-Gautier, Quentin Duez, Jérôme Cornil, Pascal Gerbaux, and Benjamin Elias*

Cite This: https://dx.doi.org/10.1021/acs.inorgchem.0c03004

Read Online

ACCESS | Metrics & More | Article Recommendations | Supporting Information

ABSTRACT: Four trinuclear ruthenium(II) polypyridyl complexes were synthesized, and a detailed investigation of their excited-state properties was performed. The tritopic sexi-pyridine bridging ligands were obtained via *para* or *meta* substitution of a central 2,2′-bipyridine fragment. A *para* connection between the 2,2′-bipyridine chelating moieties of the bridging ligand led to a red-shifted MLCT absorption band in the visible part of the spectra, whereas the *meta* connection induced a broadening of the LC transitions in the UV region. A convergent energy transfer from the two peripheral metal centers to the central Ru(II) moiety was observed for all trinuclear complexes. These complexes were in thermal equilibrium with an upper-lying ^{3}MLCT excited state over the investigated range of temperatures. For all complexes, deactivation via the ^{3}MC excited state was absent at room temperature. Importantly, the connection in the *para* position for both central and peripheral 2,2′-bipyridines of the bridging ligand resulted in a trinuclear complex ($\mathbf{T_{pp}}$) that absorbed more visible light, had a longer-lived excited state, and had a higher photoluminescence quantum yield than the parent $[Ru(bpy)_3]^{2+}$, despite its red-shifted photoluminescence. This behavior was attributed to the presence of a highly delocalized excited state for $\mathbf{T_{pp}}$.

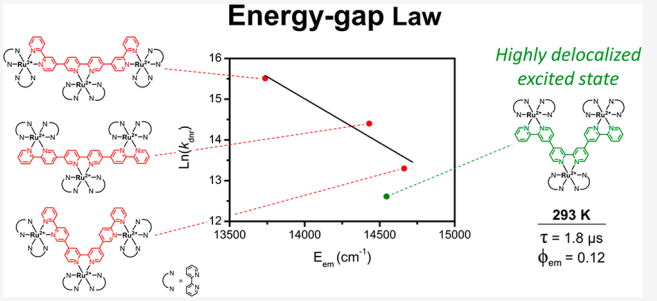

INTRODUCTION

For decades,[1,2] the interest in the photophysical and photochemical properties of $[Ru(bpy)_3]^{2+}$ and its derivatives has remained unaltered, and $[Ru(bpy)_3]^{2+}$-type complexes have found many applications in photocatalysis, artificial photosynthesis, sensing, nanoscale machines, etc.[3−6] Light absorption by $[Ru(bpy)_3]^{2+}$ predominantly occurs in the high energy portion of the solar spectrum. Increasing the light absorption at lower energy while maintaining appreciable photoluminescence (PL) and a long-lived excited state is of prime interest. A strategy to absorb light at longer wavelengths is to decrease the HOMO−LUMO energy gap which typically results in bathochromic shifts of the absorption and photoluminescence.[7,8] While this strategy allows longer wavelength light to be absorbed, the molar absorption coefficient typically remains unaltered. A promising approach to increase the molar absorption coefficient is to turn to polynuclear complexes. In addition, the bridging ligand connecting the different metal centers can display lower energy π^* acceptor orbitals and hence also induce bathochromic shifts of the MLCT absorption bands and photoluminescence.[9,10] Therefore, polynuclear complexes are prime candidates to absorb light more efficiently at longer wavelengths than mononuclear $[Ru(bpy)_3]^{2+}$-type complexes. Moreover, the red-shifted photoluminescence is accompanied by a larger direct non-radiative deactivation rate constant (k_{dnr}) to the ground state, as predicted by the energy-gap law, and consequently yields shorter excited-state lifetimes.[11−14] This drawback can be partially prevented in polynuclear complexes by judicious bridging ligand design, in which a more delocalized excited state results in a smaller k_{dnr}.[15−22] Dinuclear Ru(II) complexes based on a ditopic bridging ligand were far more thoroughly investigated[23] compared to trinuclear Ru(II) complexes based on a tritopic bridging ligand. Most of the tritopic ligands described in the literature are comprised of bi- or tridentate polypyridyl chelating moieties and can be separated into two categories: tritopic ligands with chemically equivalent binding sites[9,24−30] and tritopic ligands with at least one chemically inequivalent binding site.[31−40] In the latter case, although all Ru(II) centers have identical ancillary ligands, an efficient convergent energy transfer could be evidenced (molecular antenna).[31,34,36−38,41] Surprisingly, in this category, most of the reported examples are based on tritopic ligands with terpyridine-type binding sites, whereas bipyridine-based tritopic bridging ligands remain scarcely studied.[41]

Received: October 9, 2020

Scheme 1. Synthetic Scheme of the Desired Ligands (L_{pp}, L_{pm}, L_{mp}, L_{mm}), Complexes (T_{pp}, T_{pm}, T_{mp},T_{mm}), and Structures of the Related Dinuclear Complexes (D_p, D_m)[a,b]

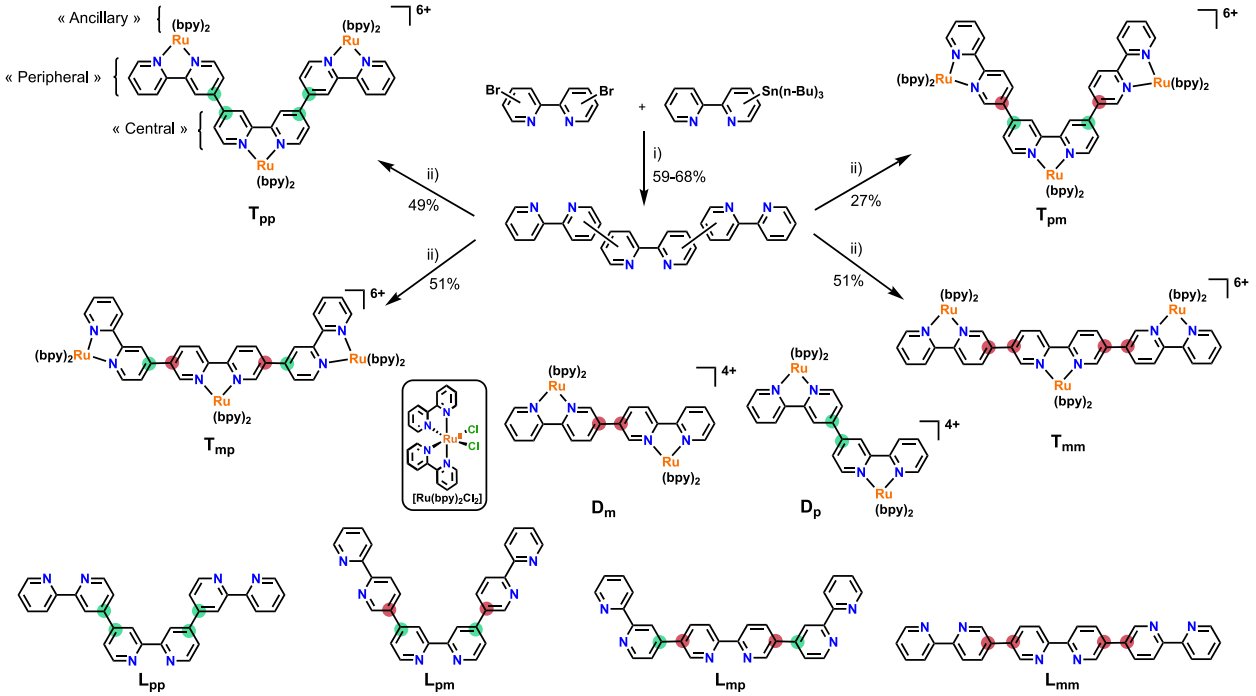

[a](i) $[Pd(PPh_3)_4]$, toluene, argon, 6 days, 135 °C; (ii) $[Ru(bpy)_2Cl_2]$, $AgNO_3$, $(CH_2OH)_2/H_2O$: 9/1, 180 °C, MW, 1 h. [b]Green and red circles indicate *para* and *meta* substitutions, respectively.

In this study, different strategies for assembling three $[Ru(bpy)_3]^{2+}$ subunits into trinuclear complexes were investigated and the photophysical properties of the resulting complexes were studied. The four trinuclear Ru(II) complexes are based on tritopic sexi-pyridine bridging ligands and six 2,2′-bipyridine (bpy) ancillary ligands (Scheme 1). The different bridging ligands investigated are composed of two peripheral 2,2′-bipyridine moieties connected to a central 2,2′-bipyridine moiety. Connections between the bipyridines were varied between the *meta* and *para* positions for the central as well as for the peripheral bipyridine moieties, resulting in four regioisomeric, tritopic ligands (Scheme 1). For the sake of clarity, the resulting complexes are termed "T" for trinuclear, followed by "p" or "m" for *para* or *meta* substitution, respectively. The first substitution letter stands for the modification of the central 2,2′-bipyridine, while the second letter corresponds to the modification of the peripheral 2,2′-bipyridine.

The four trinuclear complexes were characterized by UV−visible absorption spectroscopy, cyclic and differential pulsed voltammetry, as well as by steady-state and time-resolved photoluminescence over a wide range of temperatures. The experimental results reported herein indicate that the geometry of the bridging ligand and therefore the connection between the Ru(II) subunits play a decisive role in the photophysical properties. Strikingly, the connection of three 2,2′-bipyridine fragments via the *para* position (4,4′) resulted in a complex (T_{pp}) that absorbed more visible light at longer wavelengths and exhibited a longer excited-state lifetime and a higher photoluminescence quantum yield than the parent $[Ru(bpy)_3]^{2+}$ complex. The other bridging ligands yielded trinuclear complexes (T_{pm}, T_{mp}, T_{mm}) that exhibited excited-state lifetimes and photoluminescence quantum yields smaller than $[Ru(bpy)_3]^{2+}$.

RESULT AND DISCUSSION

Synthesis and Characterization. The four tritopic sexi-pyridine ligands, L_{pp}, L_{pm}, L_{mp}, and L_{mm}, were synthesized through a Stille coupling between 4- or 5-(tributylstannyl)-2,2′-bipyridine and 4,4′- or 5,5′-dibromo-2,2′-bipyridine in the presence of $[Pd(PPh_3)_4]$ (Scheme 1). The corresponding complexes, T_{pp}, T_{pm}, T_{mp}, and T_{mm}, were synthesized by heating the corresponding tritopic ligand with an excess of $[Ru(bpy)_2Cl_2]$ in the presence of silver nitrate in an ethylene glycol/water mixture for 1 h at 180 °C under microwave irradiation. The complexes were purified by column chromatography on silica gel and isolated as hexafluorophosphate salts after ion metathesis. The four complexes were present as a mixture of stereoisomers, complicating ^{1}H NMR characterization. The chemical composition of the trinuclear complexes was confirmed by high resolution mass spectrometry (HRMS) using electrospray ionization (ESI). The recorded mass spectra featured a series of well-defined peaks corresponding to adducts of the trinuclear complexes with PF_6^- counterions with charged states ranging from 2+ to 6+ (Figure 1A and Figures S19−S34). Since the four trinuclear complexes are regioisomers, they have the same chemical composition and m/z ratios, resulting in identical mass distributions. In order to ensure the regioisomeric purity of each compound, ESI-MS was associated with traveling wave ion mobility spectrometry (TWIMS).[42,43] TWIMS is an experimental technique that allows for separation of ions based on their mobility in a cell filled with a buffer gas (He or N_2) under an applied electric field. The drift time spent in such a mobility cell is directly proportional to the ion collisional

https://dx.doi.org/10.1021/acs.inorgchem.0c03004
Inorg. Chem. XXXX, XXX, XXX−XXX

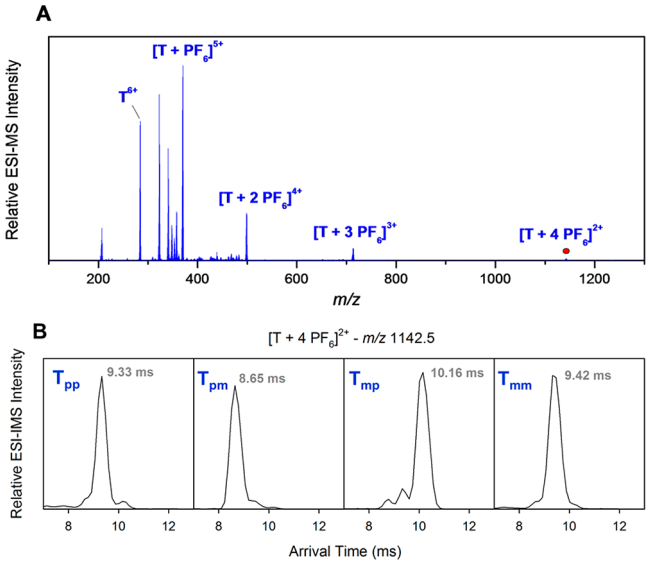

Figure 1. (A) Representative ESI-MS spectrum of a trinuclear complex. Adducts of T with PF_6^- counterions are highlighted. (B) Arrival time distributions recorded for m/z 1142.5, corresponding to $[T + 4\ PF_6]^{2+}$ (red dot) for each trinuclear complex.

cross section (CCS), which is associated with the 3D structure of the complex. The four trinuclear complexes were characterized by ESI-TWIMS-MS in their 2+ charged state (i.e., with four PF_6^- counterions). All four trinuclear complexes exhibited a narrow and unimodal arrival time distribution (ATD). However, the four regioisomeric complexes displayed a distinct time distribution (Figure 1) arising from the different 3D structures in the gas phase, which points to the regioisomeric purity of the four complexes. In order to gain more insights into the spatial structure of each complex, molecular dynamics (MD) simulations were performed to generate candidate structures for each system. The theoretical average values of the associated collisional cross sections were in good agreement with the experimental values (less than 3% difference, Table 1). The corresponding ion structures are reported in Figure S35.

Table 1. Experimental and Theoretical Collisional Cross Sections Derived from TWIMS-MS Experiments and Molecular Dynamics Simulations, Respectively[a]

complex	experimental CCS (Å^2)	theoretical CCS (Å^2)
$\mathbf{T_{pp}}$	370.2 ± 1.3	374.4 ± 3.4
$\mathbf{T_{pm}}$	353.4 ± 0.6	361.8 ± 3.0
$\mathbf{T_{mp}}$	391.1 ± 0.7	395.8 ± 2.8
$\mathbf{T_{mm}}$	372.6 ± 1.1	379.2 ± 3.0

[a]Experimental values are averaged over three separate experiments, whereas theoretical values are averaged over 250 candidate structures extracted from MD simulations. Errors correspond to standard deviations.

Ground-State Properties. The electrochemical properties of the complexes were investigated by cyclic and differential pulse voltammetry (Figures S36 and S37), and the corresponding data are gathered in Table 2. The observation of a single three-electron oxidation wave at an identical potential for the four complexes indicated that the peripheral and central Ru(II) centers underwent simultaneous oxidation and hence were behaving as independent centers.[44] For Ru(II)

Table 2. Oxidation and Reduction Potentials (V vs Ag/AgCl)[c]

complex	$E_{1/2}(Ru^{III/II})$[a] (V vs Ag/AgCl)	$E_{1/2}(L^{n/n-1})$[b] (V vs Ag/AgCl)			
$\mathbf{T_{pp}}$	+1.38	−0.93	−1.09	−1.45	−1.59
$\mathbf{T_{pm}}$	+1.38	−0.93	−1.02	−1.25	−1.44
$\mathbf{T_{mp}}$	+1.38	−0.78	−0.94	−1.43	−1.59
$\mathbf{T_{mm}}$	+1.38	−0.86	−0.96	−1.44	−1.54
$[Ru(bpy)_3]^{2+}$	+1.30	−1.31	−1.50	−1.75	

[a]Cyclic voltammetry in acetonitrile. [b]Differential pulse voltammetry in DMF. [c]Redox potentials can be estimated vs NHE by adding 0.2 V.

polypyridyl complexes, it is usually accepted that the reduction processes are ligand-centered.[45] The first two one-electron reduction events were attributed to reductions of the bridging ligand, upon comparison with the parent complex $[Ru(bpy)_3]^{2+}$. The geometry of the bridging ligand strongly influenced the reduction patterns of the trinuclear complexes. The first reduction occurred at more positive potentials when the central bipyridine of the bridging ligand was connected via the *meta* (5,5′) position ($\mathbf{T_{mp}}$, $\mathbf{T_{mm}}$) compared to a connection via the *para* (4,4′) position ($\mathbf{T_{pp}}$, $\mathbf{T_{pm}}$). Hence, this first reduction was attributed to a central 2,2′-bipyridine-based reduction.[46,47] Both $\mathbf{T_{pp}}$ and $\mathbf{T_{pm}}$ exhibited similar potentials for the first ligand-centered reduction. For complexes with a central bipyridine substituted in the *meta* position, a *para* substitution of the peripheral bipyridines ($\mathbf{T_{mp}}$) resulted in a complex that was more easily reduced than the *meta*-substituted ones ($\mathbf{T_{mm}}$). The second reduction wave appeared to be controlled by the substitution of the peripheral bipyridine of the bridging ligand. Indeed, in the complexes where these peripheral bipyridines were connected via the *meta* position to the central one ($\mathbf{T_{pm}}$, $\mathbf{T_{mm}}$), a smaller difference in redox potential between the first and the second reduction waves (90−100 mV) was observed in comparison to the complexes where the peripheral bipyridines were connected to the central one via their *para* position ($\mathbf{T_{pp}}$, $\mathbf{T_{mp}}$, 160 mV).[16] The second reduction process was therefore attributed to the reduction of one peripheral bipyridine of the bridging ligand.

The ground-state absorption spectra of the complexes are shown in Figure 2a, and the absorption band maxima are gathered in Table 3. The absorption spectra are typical of Ru(II) polypyridyl complexes.[45] The intense absorption bands in the UV region were attributed to ligand-centered transitions, and those recorded between 400 and 550 nm were due to spin-allowed metal-to-ligand charge transfer (^{1}MLCT) transitions. The absorption spectra of the four trinuclear complexes did not simply represent a 3-fold increase of the $[Ru(bpy)_3]^{2+}$ absorption spectra (Figure S38), as would be expected for three non-interacting $[Ru(bpy)_3]^{2+}$ fragments, but rather, displayed new optical transitions. In the UV region, a broadening of the $\pi\rightarrow\pi^*$ ligand-centered transition around 290 nm was observed and became more pronounced as the number of linearly arranged pyridine moieties increased ($\mathbf{T_{mm}}$ > $\mathbf{T_{mp}}$ > $\mathbf{T_{pm}}$ > $\mathbf{T_{pp}}$). In the case of $\mathbf{T_{mm}}$, where six pyridine moieties are arranged in a linear orientation, a new distinct transition appeared at 336 nm. For the ^{1}MLCT transitions, $\mathbf{T_{pp}}$, $\mathbf{T_{pm}}$, and $\mathbf{T_{mp}}$ exhibited two distinct transition bands, one centered at a similar energy as for $[Ru(bpy)_3]^{2+}$ (~450 nm) and a second at lower energy (~480 nm). $\mathbf{T_{mm}}$, on the other hand, only displayed one transition band at higher energy. The

https://dx.doi.org/10.1021/acs.inorgchem.0c03004
Inorg. Chem. XXXX, XXX, XXX−XXX

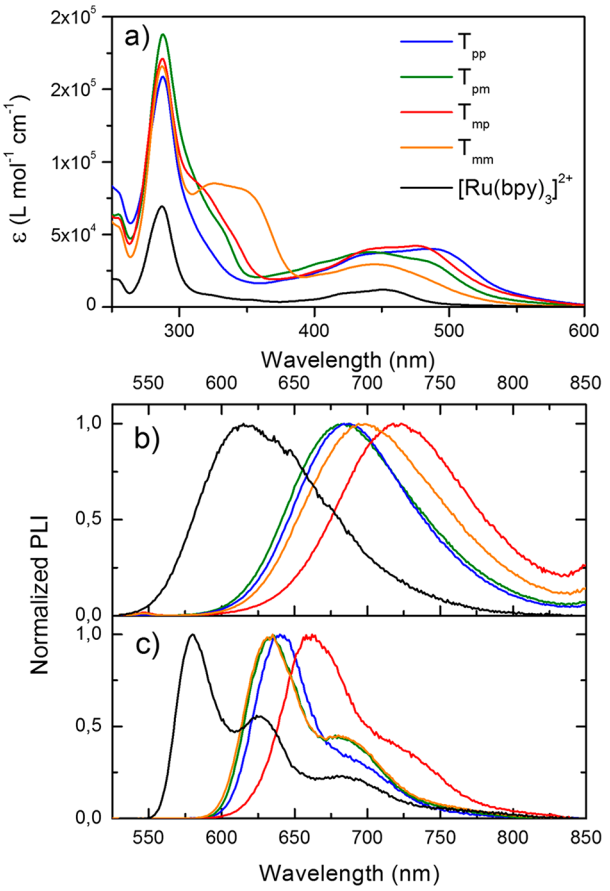

Figure 2. UV−visible absorption spectra for the complexes in acetonitrile at 293 K (a). Normalized steady-state photoluminescence spectra of the complexes in acetonitrile solution at 293 K (b) and in butyronitrile rigid matrix at 77 K (c).

transitions at 450 nm were attributed to ^{1}MLCT transitions from the Ru(II) centers to orbitals localized on the external 2,2′-bipyridine (bpy) ancillary ligands, as well as orbitals localized on the bridging ligands. The ^{1}MLCT transition at 480 nm only involved the bridging ligands.[48] The molar absorption coefficients associated with the transitions at 480 nm increased as the number of *para*-connected 2,2′-bipyridines on the bridging ligand increased, such that $\mathbf{T_{pp}} > \mathbf{T_{mp}} > \mathbf{T_{pm}}$. This agreed with previous observations of complexes with 2,2′-bipyridine ligands substituted in the 4,4′ positions that exhibited more intense ^{1}MLCT transitions than their corresponding complexes substituted in the 5,5′ positions.[46,49] All trinuclear complexes reported herein exhibited molar absorption coefficients for the ^{1}MLCT transitions appreciably larger than that of $[Ru(bpy)_3]^{2+}$ (Figures 2 and S38).

A correlation between the energy of the most bathochromic distinct ^{1}MLCT transition and the energy associated with the redox process ($\Delta E_{1/2} = E_{1/2}(Ru^{III/II}) - E_{1/2}(L^{n/n-1})$), also known as spectroelectrochemical correlation,[8,50] was observed for the *para*-substituted derivatives, $\mathbf{T_{pp}}$ and $\mathbf{T_{pm}}$ (Figure S40), indicating that the same orbitals were involved in both the electrochemical and photophysical processes. For the *meta*-substituted derivatives, i.e., $\mathbf{T_{mp}}$ and $\mathbf{T_{mm}}$, the absence of correlation most probably originates from the fact that the first ligand-centered reduction process occurs on the central 2,2′-bipyridine moiety of the bridging ligand and its *meta* substitution results in a ^{1}MLCT transition with moderate oscillator strength. As a result, the intensity of the ^{1}MLCT transition correlated to the first reduction and oxidation processes could be too weak to appear as a distinct feature or could even be hidden in the tail of the transitions occurring at higher energy.

Excited-State Properties. At 77 K, in a rigid matrix, as well as at 293 K in fluid solution, all trinuclear complexes exhibited photoluminescence with a single exponential excited-state lifetime. The trinuclear complexes are composed of two types of Ru(II) centers, i.e., two peripheral and one central. The experimental observation of one single exponential luminescent lifetime indicated that the photoluminescence arose from only one type of Ru(II) center. This was made possible by an energy transfer between the two types of Ru(II) centers, and supported by the close match between the absorption and excitation spectra (Figures S41−S44). The photoluminescence of related dinuclear complexes $\mathbf{D_p}$ and $\mathbf{D_m}$[10] (Scheme 1) was recorded at higher energy than for the corresponding trinuclear complexes, both at 77 and 293 K. The red-shifted photoluminescence of the trinuclear complexes compared to the dinuclear analogue strongly suggested that, in the trinuclear complexes, a convergent energy transfer is taking place from the peripheral Ru(II) to the central Ru(II) subunits. Hence, it was proposed that the ^{3}MLCT excited state responsible for the photoluminescence corresponded to a charge transfer between the central bipyridine moiety and the central Ru center. Franck−Condon line-shape analysis of the

Table 3. Photophysical Properties of the Trinuclear Complexes and $[Ru(bpy)_3]^{2+}$

	absorption	luminescence						
	293 K[a]	293 K[a]					77 K[g]	
complex	λ_{max} (nm); ε (M^{-1} cm^{-1})	λ_{max} (nm)[b]	τ (ns)[c]	Φ_{PL}[c,d]	k_r[c,e] (10^4 s^{-1})	k_{nr}[c,f] (10^6 s^{-1})	λ_{max} (nm)[b]	τ (μs)
$\mathbf{T_{pp}}$	484 (40100), 440 (36600), 288 (158800)	684	1815 (345)	0.121 (0.022)	6.7	0.5	641	6.2
$\mathbf{T_{pm}}$	485 (31200), 442 (37800), 288 (188000)	683	623 (224)	0.048 (0.017)	7.7	1.5	635	4.6
$\mathbf{T_{mp}}$	475 (42200), 450 (40800), 287 (171100)	721	298 (117)	0.0095 (0.0028)	3.2	3.3	662	2.6
$\mathbf{T_{mm}}$	445 (29500), 326 (85200), 287 (166100)	698	312 (175)	0.014 (0.0089)	4.5	3.2	633	3.4
$[Ru(bpy)_3]^{2+}$[h]	450 (12000), 287 (69400)	615	890 (170)	0.094 (0.018)	11.0	1.0	579	4.8

[a]Acetonitrile solution. [b]Excitation at 450 nm. [c]In argon purged acetonitrile solution with values for air-equilibrated solution in parentheses; uncertainties are estimated to be 5%. [d]$[Ru(bpy)_3]^{2+}$ in air-equilibrated acetonitrile used as reference (Φ_{PL} = 0.018);[51] uncertainties are estimated to be 10%. [e]$k_r = \Phi_{em}/\tau$. [f]$\tau = 1/(k_r + k_{nr})$. [g]Butyronitrile rigid matrix. [h]From ref 10.

https://dx.doi.org/10.1021/acs.inorgchem.0c03004
Inorg. Chem. XXXX, XXX, XXX−XXX

photoluminescence recorded at 77 K (Figures S45–S48) yielded better insight into the excited-state properties. The photoluminescence spectra were fit according to eq 1, where E_0 corresponds to the energy difference between the ground- and excited-state potential energy surfaces in their zeroth vibrational level, S_M is the Huang–Rhys factor, also known as the coupling factor that gauges the geometric distortion between the ground and excited states, $\hbar\omega_M$ corresponds to the vibrational energy spacing in the ground-state potential energy surface for the mode contributing the most to the geometric distortion, and $\Delta\nu_{1/2}$ is the full-width at half-maximum of the transition (fwhm).[52,53] The extracted data are gathered in Table 4.

$$I(\tilde{\nu}) = \sum_{\nu_m=0}^{\infty}\left[\left(\frac{E_0 - \nu_m\hbar\omega_M}{E_0}\right)^3 * \frac{S_M^{\nu_m}}{\nu_m!} * \exp\left\{-4\ln 2\left[\frac{\tilde{\nu} - E_0 + \nu_m\hbar\omega_M}{\Delta\nu_{1/2}}\right]^2\right\}\right] \quad (1)$$

Table 4. Fitting Parameters Obtained from the Franck–Condon Line-Shape Analysis[a]

complex	E_0 (cm^{-1})	$\hbar\omega_M$ (cm^{-1})	S_M	fwhm (cm^{-1})
$\mathbf{T_{pp}}$	15650	1170	0.33	1010
$\mathbf{T_{pm}}$	15790	1190	0.46	990
$\mathbf{T_{mp}}$	15140	1220	0.39	1160
$\mathbf{T_{mm}}$	15820	1220	0.47	1020

[a]At 77 K in butyronitrile rigid matrix; no parameters were constrained for the fitting calculations.

The vibrational modes ($\hbar\omega_M$) were found to be of similar magnitude for all complexes, i.e., 1170–1220 cm^{-1}. These values were in good agreement with that of an average acceptor vibrational mode of C–C and C–N stretches in polypyridine-type ligands, as already stated in the literature.[54,55,53,56] Despite small differences in E_0 (~15600–15800 cm^{-1}), $\mathbf{T_{pp}}$ exhibited a significantly smaller Huang–Rhys factor (S_M) than $\mathbf{T_{pm}}$ and $\mathbf{T_{mm}}$, indicating a more delocalized excited state in $\mathbf{T_{pp}}$.[16−19] A delocalized excited state suggested that the excited electron was delocalized over a large molecular framework, which decreases the amplitude of geometric distortions of the C–C and C–N bonds.[15] Consequently, the excited state was less distorted in comparison to the ground state, resulting in a decrease in the vibrational overlap between these two states.[18] The small S_M for $\mathbf{T_{mp}}$ could be explained by its smaller E_0, as a decrease in E_0 is usually accompanied by a concomitant decrease in the Huang–Rhys factor.[12,53,57−59] At 77 K, deactivation of the ^{3}MLCT excited state via the activated pathways to the upper-lying ^{3}MLCT and ^{3}MC excited states was negligible (vide infra), and hence, the excited-state lifetimes were determined by the activationless direct radiative (k_{dr}) and non-radiative (k_{dnr}) deactivation rate constants. The trend in excited-state lifetimes at 77 K ($\tau_{Tpp} > \tau_{Tpm} > \tau_{Tmm}$) for the three complexes with similar E_0 was attributed mainly to the variation in Huang–Rhys factors ($S_M(\mathbf{T_{pp}}) < S_M(\mathbf{T_{pm}}) < S_M(\mathbf{T_{mm}})$), as k_{dnr} increases when S_M increases.[18] The excited-state lifetime of $\mathbf{T_{mp}}$ was the shortest of all the trinuclear complexes, which was linked to its 600 cm^{-1} smaller E_0 value compared to the other complexes. The Englman–Jortner

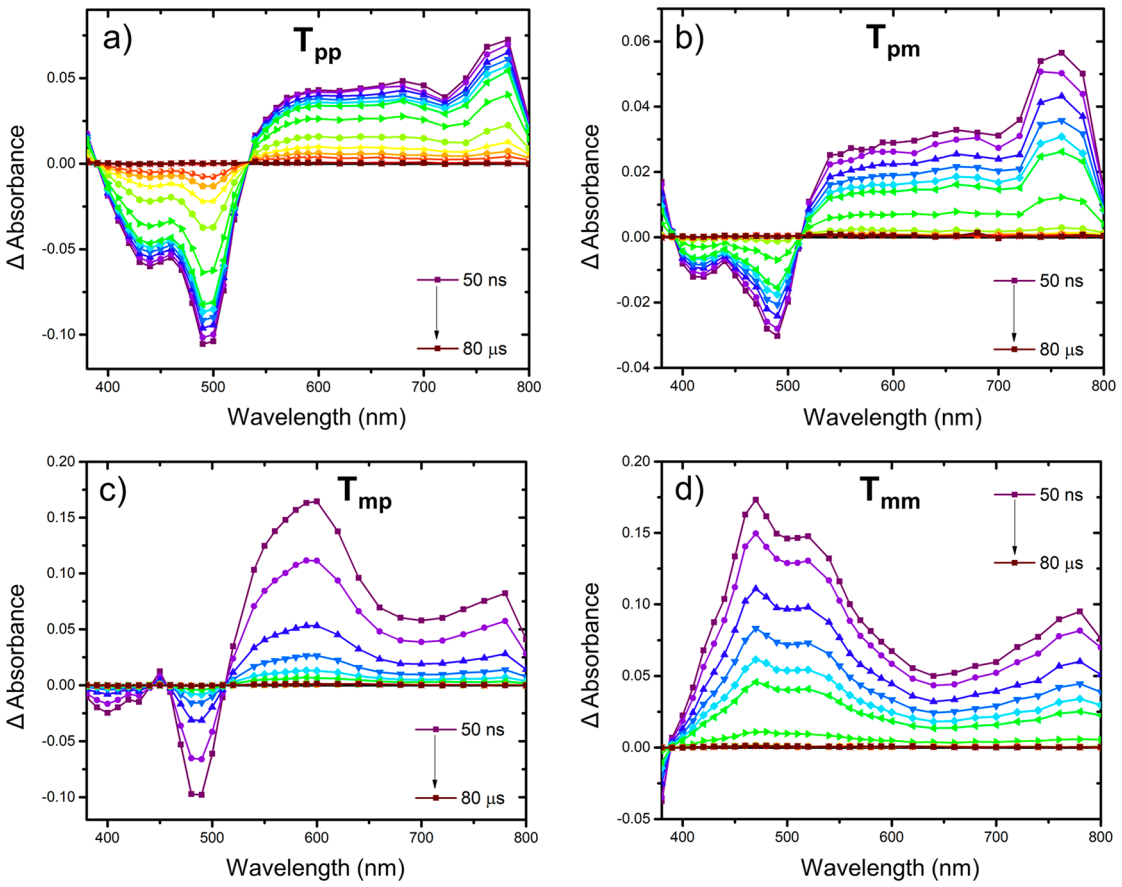

Figure 3. Transient absorption spectra at 293 K of $\mathbf{T_{pp}}$ (a), $\mathbf{T_{pm}}$ (b), $\mathbf{T_{mp}}$ (c), and $\mathbf{T_{mm}}$ (d) after pulsed 532 nm excitation in argon purged butyronitrile.

https://dx.doi.org/10.1021/acs.inorgchem.0c03004
Inorg. Chem. XXXX, XXX, XXX−XXX

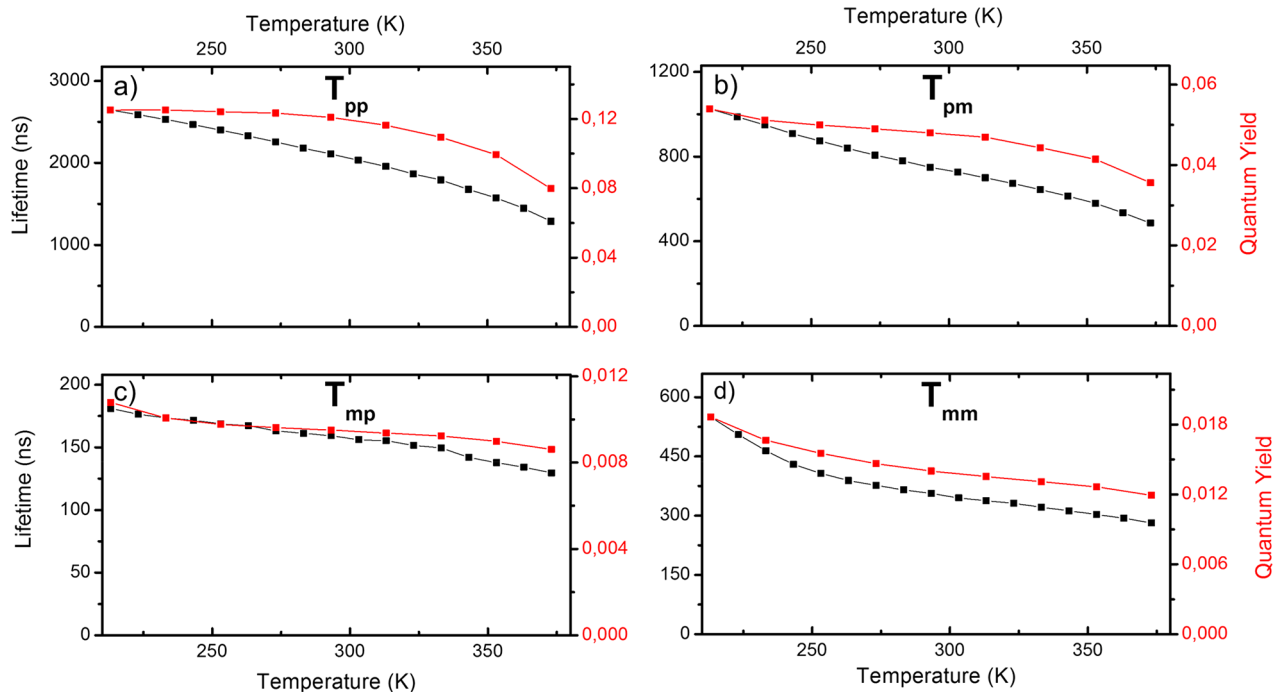

Figure 4. Photoluminescence lifetimes (black squares) and quantum yields (red squares) as a function of temperature for $\mathbf{T}_{pp}$ (a), $\mathbf{T}_{pm}$ (b), $\mathbf{T}_{mp}$ (c), and $\mathbf{T}_{mm}$ (d) in argon purged butyronitrile.

energy-gap law[11] states that, when the energy gap decreases (E_0), k_{dnr} increases and hence the excited-state lifetime is shortened.[14,58]

The change from a rigid matrix to a room temperature fluid solution was accompanied by an expected bathochromic shift of the photoluminescence maxima due to enhanced solvation effects in the fluid medium (Figure 2).[14] At 293 K, the trinuclear complexes possessing a bridging ligand with a *para*-substituted central bipyridine ($\mathbf{T}_{pp}$, $\mathbf{T}_{pm}$) exhibited photoluminescence maxima at similar wavelengths. When the central bipyridine was *meta*-substituted ($\mathbf{T}_{mp}$, $\mathbf{T}_{mm}$), red-shifted photoluminescence occurred (Figure 2). The corresponding photoluminescence lifetimes and quantum yields followed the same trend ($\mathbf{T}_{pp} > \mathbf{T}_{pm} > \mathbf{T}_{mm} > \mathbf{T}_{mp}$) as observed at 77 K. $\mathbf{T}_{pp}$ and $\mathbf{T}_{pm}$ possessed larger global radiative rate constants (k_r) than $\mathbf{T}_{mp}$ and $\mathbf{T}_{mm}$, yet these variations remained moderate. The non-radiative deactivation rate constants (k_{nr}), gathering the direct and activated deactivation pathways (k_{dnr}, k^{3}_{MLCT}, k^{3}_{MC}), exhibited a more contrasting behavior among the complexes.

For all trinuclear complexes, a correlation between the photoluminescence maxima at 293 K and the $\Delta E_{1/2}$ ($\Delta E_{1/2} = E_{1/2}(Ru^{III/II}) - E_{1/2}(L^{n/n-1})$) was noted (Figure S39), indicating that orbitals of similar nature were involved in both the electrochemical and photoluminescence processes. This agreed with a lowest energy excited state, corresponding to a charge transfer between the central Ru and the central bipyridine part of the bridging ligand.[7,8,50]

Nanosecond transient absorption spectra of the trinuclear complexes in butyronitrile at 293 K are presented in Figure 3. For all complexes, the transient absorption changes decayed according to a unimolecular process over the whole spectral range on a time scale consistent with photoluminescence lifetime measurements, attributed to deactivation of the lowest ^{3}MLCT excited state. Energy transfer between metal centers in polynuclear polypyridine complexes usually takes place on the femto- to picosecond time scale.[60−62] Hence, the energy transfer had already occurred within the time scale of the transient spectra measurements and the observed excited state corresponds therefore to the lowest ^{3}MLCT. The transient absorption spectra of $\mathbf{T}_{pp}$ were most similar to the one of $[Ru(bpy)_3]^{2+}$,[63] where the bleaching between 400 and 520 nm was attributed to the formal oxidation of Ru(II) to Ru(III) and the positive features between 520 and 800 nm were attributed to intra-ligand transitions of the formally monoreduced bridging ligand ($\mathbf{L}_{pp}^{\bullet-}$).[22,64,65] The transient absorption spectra of the three other complexes exhibited more unusual behaviors. In comparison to $\mathbf{T}_{pp}$, a moderate decrease in the 450 nm bleaching was observed for $\mathbf{T}_{pm}$. In the case of $\mathbf{T}_{mp}$, this bleach was of smaller intensity and it was completely absent for $\mathbf{T}_{mm}$ where, instead, a strong positive transient absorption was observed between 390 and 800 nm, with a maximum localized at 470 nm. This feature at 470 nm increased with the number of pyridine moieties arranged in a linear fashion within the bridging ligand ($\mathbf{T}_{mm} > \mathbf{T}_{mp} > \mathbf{T}_{pm} > \mathbf{T}_{pp}$). As in the ground-state UV−visible spectra, an increase in the number of linearly arranged pyridines induced a broadening of the $\pi \rightarrow \pi^*$ transitions localized on the bridging ligand. Therefore, it was proposed that the transient absorption centered at 470 nm was due to transitions mainly localized on the mono-reduced bridging ligand ($\mathbf{L}^{\bullet-}$), as shown experimentally and theoretically in related dinuclear complexes.[10]

Variable Temperature Photoluminescence. Steady-state and time-resolved photoluminescence measurements in butyronitrile at variable temperatures were performed in order to gain better insight into the excited-state deactivation pathways of trinuclear complexes. First, temperature dependent time-resolved photoluminescence measurements allowed identifying the different deactivation pathways from the lowest ^{3}MLCT excited state and the corresponding deactivation kinetic rate constants. Second, temperature dependent steady-state photoluminescence measurements, and more precisely

https://dx.doi.org/10.1021/acs.inorgchem.0c03004
Inorg. Chem. XXXX, XXX, XXX−XXX

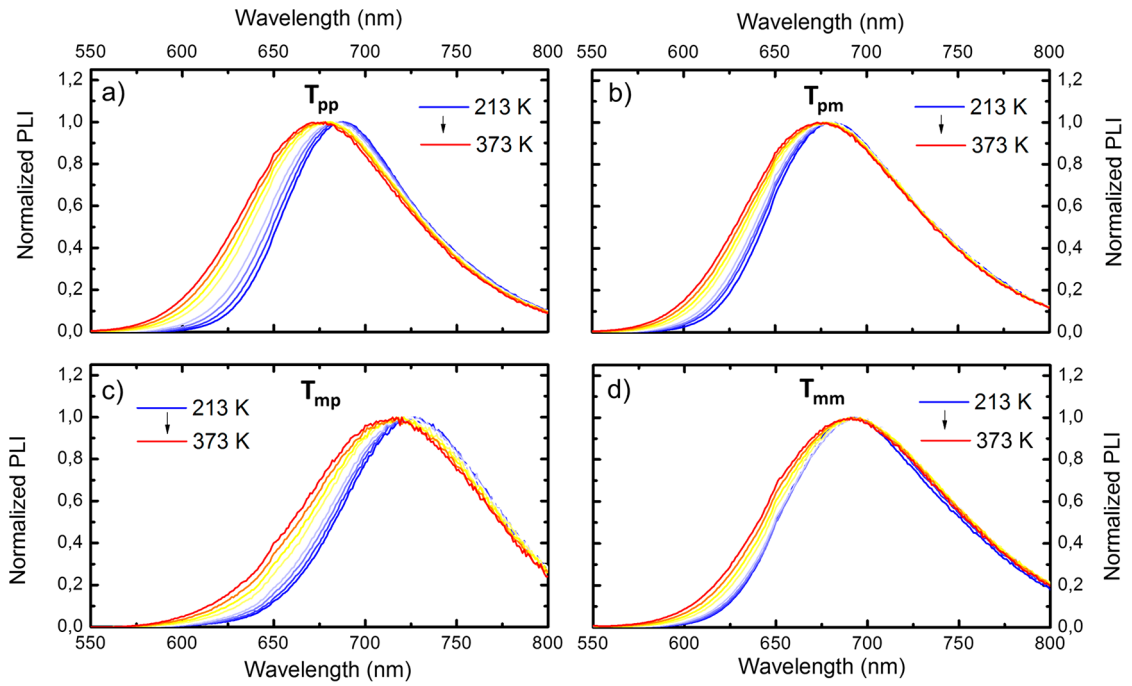

Figure 5. Normalized photoluminescence as a function of temperature for $\mathbf{T_{pp}}$ (a), $\mathbf{T_{pm}}$ (b), $\mathbf{T_{mp}}$ (c), and $\mathbf{T_{mm}}$ (d) in argon purged butyronitrile.

photoluminescence quantum yields, allowed identifying the pathways exhibiting radiative deactivation.[66,67] The observed changes in the photoluminescence lifetimes and quantum yields for each trinuclear complex are shown in Figures 4 and 5.

The photophysical scheme of the parent mononuclear complex $[Ru(bpy)_3]^{2+}$ is well established and was useful in interpreting the changes in excited-state lifetimes of the trinuclear complexes (Scheme 2).

Scheme 2. Photophysical Scheme of $[Ru(bpy)_3]^{2+}$-type Complexes with a Range of Typical Activation Energies and Pre-exponential Factors

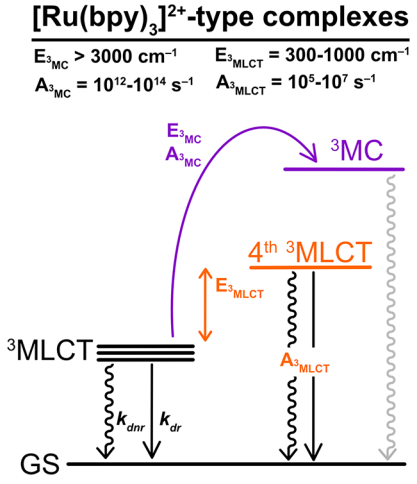

The lowest ^{3}MLCT excited state of $[Ru(bpy)_3]^{2+}$ consists of three closely lying ^{3}MLCT states in thermal equilibrium which, at temperatures greater than 77 K, behave as a single state.[66,67] This lowest ^{3}MLCT is deactivated by a direct radiative and non-radiative process to the ground state, as well as by thermally activated processes, such as the population of an upper-lying (4th) ^{3}MLCT and/or an upper-lying metal-centered state (^{3}MC).[68−70] The observed changes in photoluminescence lifetimes (τ) for the trinuclear complexes were fit according to eq 2 or 3, depending on whether deactivation through the ^{3}MC was observed, in addition to the deactivation via the upper-lying ^{3}MLCT.[68,71−73]

$$1/\tau = k_{dr} + k_{dnr} + k_{^3\mathrm{MLCT}} = k_{dr} + k_{dnr} + A_{^3\mathrm{MLCT}} e^{-E_{^3\mathrm{MLCT}}/\mathrm{RT}} \quad (2)$$

$$1/\tau = k_{dr} + k_{dnr} + k_{^3\mathrm{MLCT}} + k_{^3\mathrm{MC}} = k_{dr} + k_{dnr} + A_{^3\mathrm{MLCT}} e^{-E_{^3\mathrm{MLCT}}/\mathrm{RT}} + A_{^3\mathrm{MC}} e^{-E_{^3\mathrm{MC}}/\mathrm{RT}} \quad (3)$$

In these equations, k_{dr} and k_{dnr} are the activationless direct radiative and non-radiative decay rate constants from the three closely lying ^{3}MLCT excited states to the ground state, considered to remain constant over the range of temperatures studied.[68] The three lowest ^{3}MLCT excited states were in thermal equilibrium with the 4th upper-lying ^{3}MLCT excited state ($^3\mathrm{MLCT}_{\mathrm{lowest}} \leftrightarrow {}^3\mathrm{MLCT}_{\mathrm{upper}}$). Deactivation through the reversible thermal population of the 4th upper-lying ^{3}MLCT is associated with the rate constant $k_{^3\mathrm{MLCT}}$, with a small activation energy ($E_{^3\mathrm{MLCT}} \sim 300-1000$ cm^{-1}) and small pre-exponential factor ($A_{^3\mathrm{MLCT}} \sim 10^5-10^7$ s^{-1}).[68,74] The energy of activation $E_{^3\mathrm{MLCT}}$ corresponded to the energy gap between these states (Scheme 2), and the pre-exponential factor $A_{^3\mathrm{MLCT}}$ corresponded to the sum of the radiative and non-radiative decay rate constants from the upper-lying ^{3}MLCT excited state to the ground state.[9,75,68] In eq 3, deactivation through the ^{3}MC has been considered, which comes from the reversible or irreversible[75] thermal population of the ^{3}MC excited state. This population was associated with the rate constant $k_{^3\mathrm{MC}}$ and exhibited a large activation energy ($E_{^3\mathrm{MC}} > 3000$ cm^{-1}) and pre-exponential factor ($A_{^3\mathrm{MC}} \sim 10^{12}-10^{14}$ s^{-1}).[7,72] For this pathway, the pre-exponential factor $A_{^3\mathrm{MC}}$ was associated with high frequency vibrations whose activation led to the

https://dx.doi.org/10.1021/acs.inorgchem.0c03004
Inorg. Chem. XXXX, XXX, XXX−XXX

Table 5. Kinetic Parameters for the Excited-State Decay in Argon Purged Butyronitrile

complex	$k_{dr}+k_{dnr}$ (s^{-1})	A^{3}_{MLCT} (s^{-1})	E^{3}_{MLCT} (cm^{-1})	A^{3}_{MC} (s^{-1})	E^{3}_{MC} (cm^{-1})
$\mathbf{T_{pp}}$ [a]	3.5×10^5	5.1×10^6	750	1.2×10^{13}	4720
$\mathbf{T_{pm}}$ [a]	6.3×10^5	4.7×10^6	390	1.5×10^{13}	4540
$\mathbf{T_{mp}}$ [a]	5.5×10^6	8.4×10^7	960	[d]	[d]
$\mathbf{T_{mm}}$ [b]	1.8×10^6	1.2×10^7	510	[d]	[d]
$[Ru(bpy)_3]^{2+}$ [c]	4.1×10^5	2.6×10^6	500	1.1×10^{13}	3460

[a]Temperature range for the fitting was 213−373 K. [b]Temperature range for the fitting was 253−373 K. [c]From ref 10. [d]Not observed.

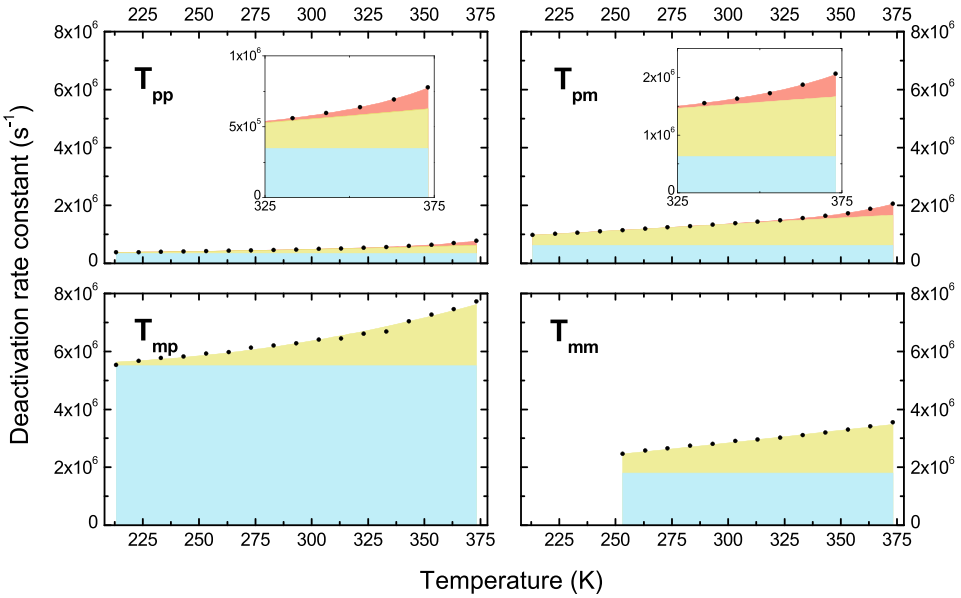

Figure 6. Excited-state deactivation rate constants for the trinuclear complexes: (blue) direct radiative and non-radiative rate constants ($k_{dr} + k_{dnr}$), (yellow) thermally activated deactivation via the upper-lying ^{3}MLCT (k^{3}_{MLCT}), (red) thermally activated deactivation pathway via the upper-lying ^{3}MC (k^{3}_{MC}) and (dot) experimental data.

Table 6. Luminescence Quantum Yield for the Different ^{3}MLCT Excited States of Each Trinuclear Complex

complex	Φ ^{3}MLCT ($k_{dr}/k_{dr}+k_{dnr}$)	k_{dr} (s^{-1})	k_{dnr} (s^{-1})	Φ ^{3}MLCT thermally activated ($A^{3}_{MLCT\ radiative}/A^{3}_{MLCT}$)
$\mathbf{T_{pp}}$	0.13 ± 0.01	4.6×10^4	3.0×10^5	0.07 ± 0.01
$\mathbf{T_{pm}}$	0.065 ± 0.005	4.1×10^4	5.9×10^5	0.030 ± 0.005
$\mathbf{T_{mp}}$	0.010 ± 0.001	5.6×10^4	5.4×10^6	0.004 ± 0.002
$\mathbf{T_{mm}}$	0.020 ± 0.002	3.6×10^4	1.8×10^6	0.004 ± 0.002

^{3}MLCT-^{3}MC surface crossing and E^{3}_{MC} represents therefore the activation energy to reach the surface crossing point. The parameters extracted from eqs 2 and 3 are gathered in Table 5, and the corresponding excited-state deactivation rate constants for each trinuclear complex are shown in Figure 6, as a function of temperature.

Within the trinuclear complexes, an energy transfer occurred from the peripheral ruthenium subunits to the central ruthenium subunits, which was followed by photoluminescence from a ^{3}MLCT excited state centered on the central ruthenium and the central bipyridine part of the bridging ligand.

Deactivation via an upper-lying ^{3}MLCT excited state (k^{3}_{MLCT}) was observed for all trinuclear complexes over the whole range of temperatures investigated. The deactivation rate constant A^{3}_{MLCT} from the upper-lying ^{3}MLCT was 1 order of magnitude faster than that from the lowest ^{3}MLCT ($k_{dr} + k_{dnr}$) as is usually observed for this class of compounds ($A^{3}_{MLCT}/k_{dr} + k_{dnr} \approx 10$).[68] The upper-lying ^{3}MLCT excited state exhibited a smaller deactivation rate constant for $\mathbf{T_{pp}}$ and $\mathbf{T_{pm}}$ than for $\mathbf{T_{mp}}$ and $\mathbf{T_{mm}}$ (Table 5). Surprisingly, the energy gap between the two ^{3}MLCT excited states was more influenced by the substitution of the *peripheral* bipyridines of the bridging ligand. When the latter were *para*-substituted ($\mathbf{T_{pp}}$ and $\mathbf{T_{mp}}$), the energy gap (E^{3}_{MLCT}) was approximately twice as large as that for *meta* substitution ($\mathbf{T_{pm}}$ and $\mathbf{T_{mm}}$). Therefore, complexes with *para*-substituted peripheral bipyridines ($\mathbf{T_{pp}}$, $\mathbf{T_{mp}}$) underwent proportionally less deactivation through the upper ^{3}MLCT than $\mathbf{T_{pm}}$, $\mathbf{T_{mm}}$. Both effects combined resulted in a significantly lower k^{3}_{MLCT} for $\mathbf{T_{pp}}$ in comparison to the other trinuclear complexes (Figure 6).

For the complexes with the *central* bipyridine substituted in the *para* position ($\mathbf{T_{pp}}$, $\mathbf{T_{pm}}$), an additional deactivation pathway via the ^{3}MC excited state was observed, but it was only significant at temperatures higher than 350 K (Figure 6).[75] The pre-exponential factor was similar ($A^{3}_{MC} \approx 10^{13}$ s^{-1}) for the two complexes, and the activation energy (E^{3}_{MC}) for $\mathbf{T_{pm}}$ was around 200 cm^{-1} smaller than that of $\mathbf{T_{pp}}$. It is well-known that a stabilization of the lowest ^{3}MLCT excited state usually results in an increase of the energy gap (E^{3}_{MC}).[9,76,77] This explained our inability to observe deactivation through

https://dx.doi.org/10.1021/acs.inorgchem.0c03004
Inorg. Chem. XXXX, XXX, XXX−XXX

the ^{3}MC excited state for $\mathbf{T_{mp}}$ and $\mathbf{T_{mm}}$ as their lowest ^{3}MLCT excited states were more stabilized. Thermal population of the ^{3}MC excited state usually leads to non-radiative deactivation to the ground state, as well as ligand loss.[78−82] For all the trinuclear complexes, the absence of deactivation through the ^{3}MC excited state at room temperature induced a much higher photostability in comparison to $[Ru(bpy)_3]^{2+}$.[20,71,76,83] For all trinuclear complexes, the activationless k_{dr} and k_{dnr} accounted for at least half of the excited-state decay at 293 K (Figure 6). The trinuclear complexes were only moderately or weakly photoluminescent at room temperature, such that $k_{dr} + k_{dnr} \approx k_{dnr}$. Therefore, k_{dnr} controls the excited-state lifetimes as confirmed by the determined value of k_{dnr} (vide infra, Tables 6 and S5). The values of k_{dnr} were investigated by the energy-gap law in its simplest form (eq 4).[15,17,18,53,84−86]

$$\ln(k_{dnr}) = c - \frac{\gamma E_0}{\hbar\omega_M} \tag{4}$$

$$\gamma = \ln\left(\frac{E_0}{S_M \hbar\omega_M}\right) - 1 \tag{5}$$

The variations of $\ln(k_{dnr})$ with the photoluminescence maxima in butyronitrile solution at 213 K are presented in Figure 7 for each trinuclear complex and the two related

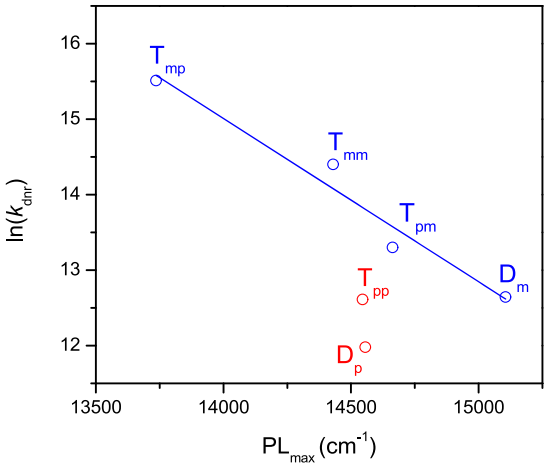

Figure 7. Energy-gap law plot of $\ln(k_{dnr})$ versus PL_{max} measured at 213 K in butyronitrile solution. The blue line represents the linear fit for $\mathbf{T_{pm}}$, $\mathbf{T_{mp}}$, $\mathbf{T_{mm}}$, and $\mathbf{D_m}$ according to eq 4 with a slope of $(-500\ cm^{-1})^{-1}$.

dinuclear complexes. Here, the PL_{max} at 213 K was used to estimate the energy gap in solution and to minimize contributions from population and photoluminescence of the upper-lying ^{3}MLCT occurring at higher temperatures.[84] A linear correlation between $\ln(k_{dnr})$ and PL_{max} was obtained for $\mathbf{T_{pm}}$, $\mathbf{T_{mp}}$, $\mathbf{T_{mm}}$, and $\mathbf{D_m}$, as suggested by eq 4. This agreed well with previous studies of a series of Ru(II) and Os(II) complexes, where the energy gap was varied by changing the non-chromophoric ligand (not implicated in the emission process).[14,53,58,84,87] In this study, the chromophoric ligand was instead varied and such a correlation was therefore interesting, as it suggested that, for the four complexes, the Huang−Rhys factor (S_M) decreased linearly with the energy gap. As a consequence, γ remained constant (eq 5), and $\hbar\omega_M$ as well as the vibronically induced electronic coupling was essentially invariant.[14,53,84,86,87]

$\mathbf{T_{pp}}$ and $\mathbf{D_p}$ did not show any correlation with the other complexes. Franck−Condon line-shape analysis of the photoluminescence spectra at 77 K revealed that both $\mathbf{T_{pp}}$ and $\mathbf{D_p}$ possessed significantly more delocalized excited states than the related dinuclear and trinuclear complexes, as was underlined by their low Huang−Rhys factors (S_M).[10] In fluid solution, at higher temperatures, the same observation was expected to hold and lower S_M values would result in smaller k_{dnr}, as revealed by eqs 4 and 5. This was previously reported in mononuclear[15,18] and polynuclear[17,19,22] complexes.

To sum up, the careful study of the different deactivation pathways from the lowest ^{3}MLCT excited states for the series of trinuclear complexes highlighted specific observations. For $\mathbf{T_{pm}}$, $\mathbf{T_{mp}}$, and $\mathbf{T_{mm}}$, k_{dnr} was governed, as expected, by the energy-gap law where a decrease in photoluminescence energy was accompanied by an increase in k_{dnr}. We propose that the excited state of $\mathbf{T_{pp}}$ is further delocalized on the bridging ligand, compared to the three other trinuclear complexes, as evidenced by its lowest S_M value. This further significantly decreased γ (eq 5) and consequently k_{dnr} (eq 4). The *para* substitution of the *peripheral* bipyridines of the bridging ligand ($\mathbf{T_{pp}}$, $\mathbf{T_{mp}}$) resulted in a larger energy gap between the lower and upper ^{3}MLCT, which in turn decreased the relative kinetic rate of deactivation via the upper ^{3}MLCT compared to the corresponding *meta*-substituted complexes ($\mathbf{T_{pm}}$, $\mathbf{T_{mm}}$). The stabilization of the lowest ^{3}MLCT increased the activation energy to the ^{3}MC which made population of that state virtually absent at 293 K for all complexes (Figure 8).

The normalized steady-state photoluminescence spectra of all trinuclear complexes exhibited a broadening of the photoluminescence band toward higher energy upon increased temperature. This broadening was accompanied by a blue shift of the photoluminescence maxima for $\mathbf{T_{pp}}$ and $\mathbf{T_{mp}}$ (Figure 5a−d). Usually, for Ru(II) polypyridyl complexes, neither a significant shift of the photoluminescence maxima or a photoluminescence band broadening is observed over the whole range of temperatures studied.[75,88,89] For all the complexes, a decrease in the excited-state lifetimes and photoluminescence quantum yields was observed when the temperature increased. However, this decrease was less pronounced for the photoluminescence quantum yield (Figure 4a−d). This can originate from an activated deactivation pathway possessing a significant contribution of radiative deactivation. The upper-lying ^{3}MLCT excited state is a prime candidate for displaying radiative deactivation to the ground state, as previously described.[10,69,89−93] Fitting the measured photoluminescence quantum yield at various temperatures ($\phi(T)$) to eq 6 or 7 allowed to determine the deactivation radiative rate constants either for the lowest ^{3}MLCT excited state or for the lowest and the upper ^{3}MLCT excited states.[10,66]

$$\phi(T) = \frac{k_{dr}}{k_{dr} + k_{dnr} + A_{^3\text{MLCT}} e^{-E_{^3\text{MLCT}}/RT} + A_{^3\text{MC}} e^{-E_{^3\text{MC}}/RT}} \tag{6}$$

$$\phi(T) = \frac{k_{dr} + A_{^3\text{MLCT radiative}} e^{-E_{^3\text{MLCT}}/RT}}{k_{dr} + k_{dnr} + A_{^3\text{MLCT}} e^{-E_{^3\text{MLCT}}/RT} + A_{^3\text{MC}} e^{-E_{^3\text{MC}}/RT}} \tag{7}$$

The parameters required for the fitting ($k_{dr} + k_{dnr}$, $A_{^3\text{MLCT}}$, $E_{^3\text{MLCT}}$, $A_{^3\text{MC}}$, and $E_{^3\text{MC}}$) are gathered in Table 5. In the case where only the lowest ^{3}MLCT exhibited significant radiative

https://dx.doi.org/10.1021/acs.inorgchem.0c03004
Inorg. Chem. XXXX, XXX, XXX−XXX

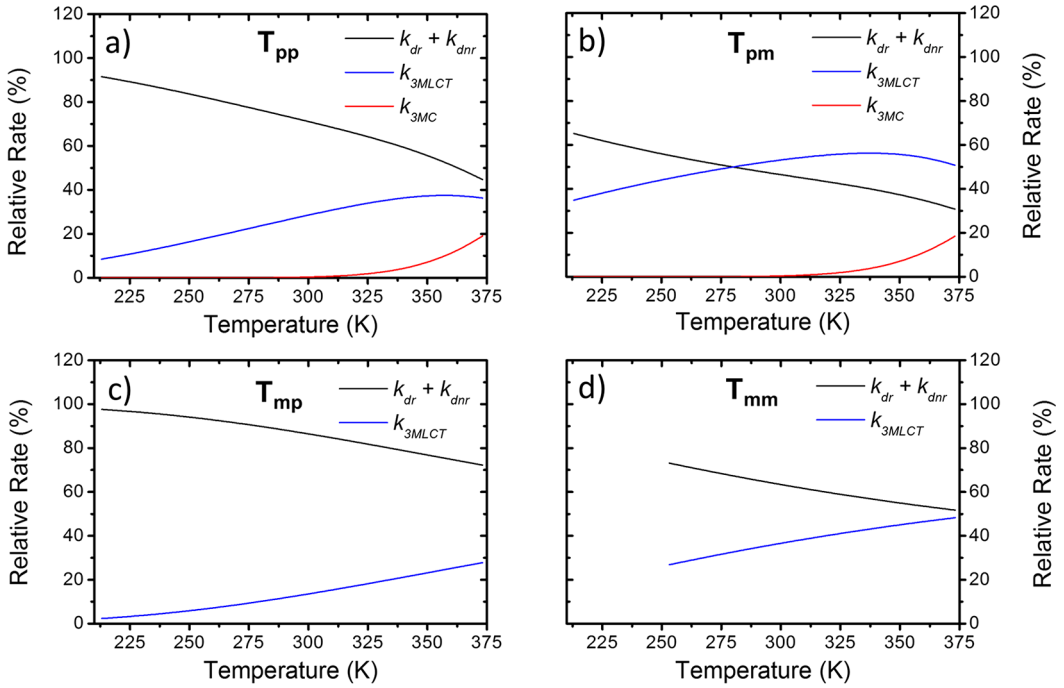

Figure 8. Relative rates of deactivation of the lowest ^{3}MLCT excited state of $\mathbf{T_{pp}}$ (a), $\mathbf{T_{pm}}$ (b), $\mathbf{T_{mp}}$ (c), and $\mathbf{T_{mm}}$ (d) via different pathways. (Black) direct radiative and non-radiative deactivation to the ground state, (blue) thermally activated deactivation through the upper-lying ^{3}MLCT excited state, and (red) thermally activated deactivation through the ^{3}MC excited state.

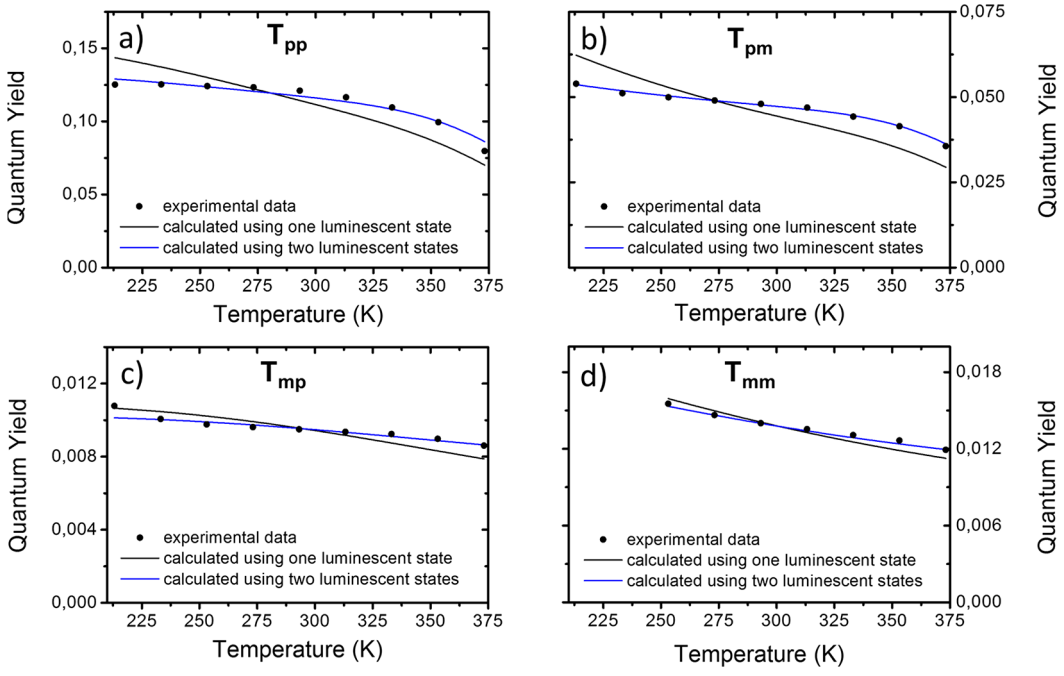

Figure 9. :Measured and calculated quantum yields of $\mathbf{T_{pp}}$ (a), $\mathbf{T_{pm}}$ (b), $\mathbf{T_{mp}}$ (c), and $\mathbf{T_{mm}}$ (d) as a function of temperature. The black dots represent the experimentally determined photoluminescence quantum yields at various temperatures. The black line represents the calculated photoluminescence quantum yields only if the lowest ^{3}MLCT excited states were luminescent. The blue line represents the calculated quantum yields if the lowest and the thermally activated ^{3}MLCT excited states were luminescent.

deactivation, the photoluminescence quantum yield was fit using eq 6 which allowed to determine k_{dr}. Equation 7 was used to determine k_{dr} and $A^{3}_{\text{MLCT radiative}}$, when both the lower- and upper-lying ^{3}MLCT excited state exhibited significant radiative deactivation. In this equation, $A^{3}_{\text{MLCT radiative}}$ corresponds to the radiative deactivation rate constant of the upper-lying ^{3}MLCT excited state to the ground state. For all trinuclear complexes, the fitting of ϕ_{PL} as a function of temperature was significantly improved when radiative deactivation from both the upper and lower ^{3}MLCT excited states was considered (Figure 9a–d). Photoluminescence originating from the upper ^{3}MLCT occurred at higher energy than from the lowest ^{3}MLCT, inducing a photoluminescence band broadening for all complexes when the temperature was

https://dx.doi.org/10.1021/acs.inorgchem.0c03004
Inorg. Chem. XXXX, XXX, XXX−XXX

increased (Figures 4 and 5).[89,90,93] The significant blue shift of the photoluminescence maxima of $\mathbf{T_{pp}}$ and $\mathbf{T_{mp}}$ originated from the larger energy gap between the lower- and upper-lying ^{3}MLCT excited states (>700 cm^{-1}) (Table 5). The photoluminescence quantum yields of the lowest ^{3}MLCT ($k_{dr}/(k_{dr} + k_{dnr})$) and upper-lying ^{3}MLCT ($A^{3}_{\mathrm{MLCT\ radiative}}/A^{3}_{\mathrm{MLCT}}$) were determined, and the results are gathered in Table 6. For all complexes, the photoluminescence quantum yield of the upper-lying ^{3}MLCT excited state was smaller than that of the lower-lying ^{3}MLCT, in agreement with the observed decrease in photoluminescence quantum yield upon temperature increase (Figure 4a–d). An approximation of the energy difference between the photoluminescence maxima of the upper and lower ^{3}MLCT was determined by deconvolution of the photoluminescence spectra of $\mathbf{T_{pp}}$ and $\mathbf{T_{mp}}$ at 213 and 373 K (Figures S57 and S58). The energy differences were, respectively, 1000 cm^{-1} for $\mathbf{T_{pp}}$ and 990 cm^{-1} for $\mathbf{T_{mp}}$, in reasonable agreement with the energy gap obtained from the analysis of the kinetic data (E^{3}_{MLCT} = 750 cm^{-1} for $\mathbf{T_{pp}}$ and E^{3}_{MLCT} = 960 cm^{-1} for $\mathbf{T_{mp}}$).[69,91,92]

CONCLUSIONS

The use of sexi-pyridine bridging ligands with non-equivalent chelating moieties induced, for all trinuclear complexes, convergent energy transfers from the two peripheral Ru(II) centers to the central Ru(II) moieties. The structures of the bridging ligands substantially influenced the photophysical properties of the resulting complexes. For the ground-state absorption properties, a *para* connection between the 2,2′-bipyridine chelating moieties of the bridging ligand yielded a bathochromic shift of the MLCT absorption bands in the visible part of the spectrum, whereas a *meta* connection induced a broadening of the LC transitions in the UV region. The excited-state properties were also strongly influenced by the bridging ligand structures, with important changes in the excited-state lifetimes. An in-depth study of the deactivation pathways as a function of temperature yielded better insight into the excited-state behavior deactivation pathways for each trinuclear complex. It was evidenced that k_{dnr} exhibited the strongest changes among the series and dominated the other deactivation pathways. For $\mathbf{T_{pm}}$, $\mathbf{T_{mm}}$, and $\mathbf{T_{mp}}$, k_{dnr} increased as the energy gap between the lowest ^{3}MLCT excited state and the ground state decreased. We propose that the smaller k_{dnr} value for $\mathbf{T_{pp}}$ (smaller than expected from the energy-gap law) originated from a more delocalized excited state over the whole bridging ligand, decreasing the displacement change and vibrational overlap, and consequently k_{dnr}.[17] The direct radiative rate constant (k_{dr}) remained similar for the trinuclear series. The excited states of the four trinuclear complexes were in thermal equilibrium with an upper-lying ^{3}MLCT excited state over the range of temperature studied. *Para* substitution of the peripheral 2,2′-bipyridines ($\mathbf{T_{pp}}$, $\mathbf{T_{mp}}$) increased E^{3}_{MLCT} between the lower and upper ^{3}MLCT compared to the *meta*-substituted complexes ($\mathbf{T_{pm}}$, $\mathbf{T_{mm}}$), resulting in a decrease of the relative rate of deactivation via the upper ^{3}MLCT ($k^{3}_{\mathrm{MLCT}}/\sum_i k_i$). For all complexes, deactivation via the ^{3}MC excited state was absent at room temperature. Indeed, stabilization of the lowest ^{3}MLCT among the series resulted in the expected increase of the activation energy (E^{3}_{MC}) for the ^{3}MLCT-^{3}MC surface crossing. Unexpected radiative deactivation from the upper-lying ^{3}MLCT excited state occurred in all trinuclear complexes reported herein. The larger energy gap between the lower and upper ^{3}MLCT (E^{3}_{MLCT}) for $\mathbf{T_{pp}}$ and $\mathbf{T_{mp}}$ induced a significant blue shift of the photoluminescence maxima upon a temperature increase. It should be mentioned that photoluminescence arising from more than one ^{3}MLCT excited state is likely more present in the literature than actually reported,[10,66,69,89−92] as time-resolved photoluminescence experiments have not always been accompanied by steady-state photoluminescence experiments.

All in all, this study underlines the striking influence of the bridging ligand geometry in polynuclear complexes. The connection in the *para* position for both central and peripheral 2,2′-bipyridines of the bridging ligand resulted in a complex, $\mathbf{T_{pp}}$, that absorbs more visible light, has a longer-lived excited state, and has a higher photoluminescence quantum yield than the parent $[Ru(bpy)_3]^{2+}$, despite having a red-shifted photoluminescence. The strategy of developing polynuclear complexes with a significantly delocalized excited state represents thus a promising strategy to obtain a low energy absorber with long-lived excited states able to perform subsequent photo-triggered chemical reactions.

ASSOCIATED CONTENT

Supporting Information

The Supporting Information is available free of charge at https://pubs.acs.org/doi/10.1021/acs.inorgchem.0c03004.

Experimental section, ^{1}H NMR, ^{13}C NMR, mass spectrometry, electrochemistry, Franck−Condon line shape analysis, and variable temperature experiments (PDF)

AUTHOR INFORMATION

Corresponding Author

Benjamin Elias − *Université catholique de Louvain (UCLouvain), Institut de la Matière Condensée et des Nanosciences (IMCN), Molecular Chemistry, Materials and Catalysis (MOST), 1348 Louvain-la-Neuve, Belgium;* orcid.org/0000-0001-5037-3313; Email: benjamin.elias@uclouvain.be

Authors

Simon Cerfontaine − *Université catholique de Louvain (UCLouvain), Institut de la Matière Condensée et des Nanosciences (IMCN), Molecular Chemistry, Materials and Catalysis (MOST), 1348 Louvain-la-Neuve, Belgium;* orcid.org/0000-0002-9865-762X

Ludovic Troian-Gautier − *Laboratoire de Chimie Organique, Université libre de Bruxelles (ULB), 1050 Brussels, Belgium; Department of Chemistry, University of North Carolina at Chapel Hill, Chapel Hill, North Carolina 27599-3290, United States;* orcid.org/0000-0002-7690-1361

Quentin Duez − *Organic Synthesis and Mass Spectrometry Laboratory, University of Mons - UMONS, B-7000 Mons, Belgium; Laboratory for Chemistry of Novel Materials, Center of Innovation and Research in Materials and Polymers (CIRMAP), University of Mons (UMONS), B-7000 Mons, Belgium;* orcid.org/0000-0002-9067-7917

Jérôme Cornil − *Laboratory for Chemistry of Novel Materials, Center of Innovation and Research in Materials and Polymers (CIRMAP), University of Mons (UMONS), B-7000 Mons, Belgium;* orcid.org/0000-0002-5479-4227

Pascal Gerbaux − *Organic Synthesis and Mass Spectrometry Laboratory, University of Mons - UMONS, B-7000 Mons, Belgium;* orcid.org/0000-0001-5114-4352

https://dx.doi.org/10.1021/acs.inorgchem.0c03004
Inorg. Chem. XXXX, XXX, XXX−XXX

Complete contact information is available at:
https://pubs.acs.org/10.1021/acs.inorgchem.0c03004

Author Contributions

The manuscript was written through contributions of all authors. All authors have given approval to the final version of the manuscript.

Notes

The authors declare no competing financial interest.

■ ACKNOWLEDGMENTS

L.T.-G. is a postdoctoral researcher of the Fonds de la Recherche Scientifique − FNRS. S.C. and B.E. gratefully acknowledge the UCLouvain for financial support. The authors acknowledge Gerald J. Meyer for the scientific generosity and providing access to his equipment. Steady-state and time-resolved absorption and photoluminescence experiments were performed using instrumentation in the CHASE Instrumentation Facility established by the Center for Hybrid Approaches in Solar Energy to Liquid Fuels, CHASE, an Energy Innovation Hub funded by the US Department of Energy, Office of Basic Energy Sciences, Office of Science, under award number DE-SC0021173. The UMONS lab is grateful to the F.R.S.-FNRS for financial support in the acquisition of the Waters Synapt G2-S*i* mass spectrometer. Q.D. is an FNRS research fellow.

■ REFERENCES

(1) Paris, J. P.; Brandt, W. W. Charge Transfer Luminescence of a Ruthenium(II) Chelate. *J. Am. Chem. Soc.* **1959**, *81*, 5001−5002.
(2) Campagna, S.; Puntoriero, F.; Nastasi, F.; Bergamini, G.; Balzani, V. In *Topics in Current Chemistry*, Vol. *280*; Balzani, V., Campagna, S., Eds.; Springer: Berlin, 2007; pp 117−214.
(3) Prier, C. K.; Rankic, D. A.; MacMillan, D. W. C. Visible Light Photoredox Catalysis with Transition Metal Complexes: Applications in Organic Synthesis. *Chem. Rev.* **2013**, *113*, 5322−5363.
(4) Troian-Gautier, L.; Turlington, M. D.; Wehlin, S. A. M.; Maurer, A. B.; Brady, M. D.; Swords, W. B.; Meyer, G. J. Halide Photoredox Chemistry. *Chem. Rev.* **2019**, *119*, 4628−4683.
(5) Valenti, G.; Rampazzo, E.; Kesarkar, S.; Genovese, D.; Fiorani, A.; Zanut, A.; Palomba, F.; Marcaccio, M.; Paolucci, F.; Prodi, L. Electrogenerated chemiluminescence from metal complexes-based nanoparticles for highly sensitive sensors applications. *Coord. Chem. Rev.* **2018**, *367*, 65−81.
(6) Baroncini, M.; Silvi, S.; Credi, A. Photo- and Redox-Driven Artificial Molecular Motors. *Chem. Rev.* **2020**, *120*, 200−268.
(7) Juris, A.; Balzani, V.; Barigelletti, F.; Campagna, S.; Belser, P.; von Zelewsky, A. Ru(II) polypyridine complexes: photophysics, photochemistry, eletrochemistry, and chemiluminescence. *Coord. Chem. Rev.* **1988**, *84*, 85−277.
(8) Barigelletti, F.; Juris, A.; Balzani, V.; Belser, P.; Von Zelewsky, A. Influence of the ligand structure on the electrochemical and spectroscopic properties of ruthenium(II)-polypyridine complexes. *Inorg. Chem.* **1987**, *26*, 4115−4119.
(9) Jacquet, L.; Mesmaeker, A. K.-D. Spectroelectrochemical characteristics and photophysics of a series of RuII complexes with 1,4,5,8,9,12-hexaazatriphenylene: effects of polycomplexation. *J. Chem. Soc., Faraday Trans.* **1992**, *88*, 2471−2480.
(10) Cerfontaine, S.; Troian-Gautier, L.; Wehlin, S. A. M.; Loiseau, F.; Cauet, E.; Elias, B. Tuning the excited-state deactivation pathways of dinuclear ruthenium(ii) 2,2′-bipyridine complexes through bridging ligand design. *Dalton Trans* **2020**, *49*, 8096−8106.
(11) Englman, R.; Jortner, J. The energy gap law for radiationless transitions in large molecules. *Mol. Phys.* **1970**, *18*, 145−164.
(12) Barqawi, K. R.; Murtaza, Z.; Meyer, T. J. Calculation of relative nonradiative decay rate constants from emission spectral profiles: polypyridyl complexes of ruthenium(II). *J. Phys. Chem.* **1991**, *95*, 47−50.
(13) Caspar, J. V.; Meyer, T. J. Application of the energy gap law to nonradiative, excited-state decay. *J. Phys. Chem.* **1983**, *87*, 952−957.
(14) Kober, E. M.; Caspar, J. V.; Lumpkin, R. S.; Meyer, T. J. Application of the energy gap law to excited-state decay of osmium(II)-polypyridine complexes: calculation of relative nonradiative decay rates from emission spectral profiles. *J. Phys. Chem.* **1986**, *90*, 3722−3734.
(15) Treadway, J. A.; Loeb, B.; Lopez, R.; Anderson, P. A.; Keene, F. R.; Meyer, T. J. Effect of Delocalization and Rigidity in the Acceptor Ligand on MLCT Excited-State Decay. *Inorg. Chem.* **1996**, *35*, 2242−2246.
(16) Boyde, S.; Strouse, G. F.; Jones, W. E.; Meyer, T. J. The effect on MLCT excited states of electronic delocalization in the acceptor ligand. *J. Am. Chem. Soc.* **1990**, *112*, 7395−7396.
(17) Strouse, G. F.; Schoonover, J. R.; Duesing, R.; Boyde, S.; Jones, W. E., Jr.; Meyer, T. J. Influence Of Electronic Delocalization In Metal-to-Ligand Charge Transfer Excited States. *Inorg. Chem.* **1995**, *34*, 473−487.
(18) Damrauer, N. H.; Boussie, T. R.; Devenney, M.; McCusker, J. K. Effects of Intraligand Electron Delocalization, Steric Tuning, and Excited-State Vibronic Coupling on the Photophysics of Aryl-Substituted Bipyridyl Complexes of Ru(II). *J. Am. Chem. Soc.* **1997**, *119*, 8253−8268.
(19) Hammarström, L.; Barigelletti, F.; Flamigni, L.; Indelli, M. T.; Armaroli, N.; Calogero, G.; Guardigli, M.; Sour, A.; Collin, J.-P.; Sauvage, J.-P. A Study on Delocalization of MLCT Excited States by Rigid Bridging Ligands in Homometallic Dinuclear Complexes of Ruthenium(II). *J. Phys. Chem. A* **1997**, *101*, 9061−9069.
(20) Cerfontaine, S.; Wehlin, S. A. M.; Elias, B.; Troian-Gautier, L. Photostable Polynuclear Ruthenium(II) Photosensitizers Competent for Dehalogenation Photoredox Catalysis at 590 nm. *J. Am. Chem. Soc.* **2020**, *142*, 5549−5555.
(21) Baba, A. I.; Ensley, H. E.; Schmehl, R. H. Influence of Bridging Ligand Unsaturation on Excited State Behavior in Mono- and Bimetallic Ruthenium(II) Diimine Complexes. *Inorg. Chem.* **1995**, *34*, 1198−1207.
(22) Grosshenny, V.; Harriman, A.; Romero, F. M.; Ziessel, R. Electron Delocalization in Ruthenium(II) and Osmium(II) 2,2′-Bipyridyl Complexes Formed from Ethynyl-Bridged Ditopic Ligands. *J. Phys. Chem.* **1996**, *100*, 17472−17484.
(23) Li, G.; Zhu, D.; Wang, X.; Su, Z.; Bryce, M. R. Dinuclear metal complexes: multifunctional properties and applications. *Chem. Soc. Rev.* **2020**, *49*, 765−838.
(24) Cheng, F.; Tang, N. Synthesis, photophysical, and electrochemical properties of two novel trinuclear Ru(II) polypyridyl complexes. *Inorg. Chem. Commun.* **2008**, *11*, 243−245.
(25) Xie, T. Z.; Liao, S. Y.; Guo, K.; Lu, X.; Dong, X.; Huang, M.; Moorefield, C. N.; Cheng, S. Z.; Liu, X.; Wesdemiotis, C.; Newkome, G. R. Construction of a highly symmetric nanosphere via a one-pot reaction of a tristerpyridine ligand with Ru(II). *J. Am. Chem. Soc.* **2014**, *136*, 8165−8.
(26) Xu, L.; Liao, G.-L.; Chen, X.; Zhao, C.-Y.; Chao, H.; Ji, L.-N. Trinuclear Ru(II) polypyridyl complexes as human telomeric quadruplex DNA stabilizers. *Inorg. Chem. Commun.* **2010**, *13*, 1050−1053.
(27) Laramée-Milette, B.; Lussier, F.; Ciofini, I.; Hanan, G. S. A family of Ru(ii) complexes built on a novel sexipyridine building block: synthesis, photophysical properties and the rare structural characterization of a triruthenium species. *Dalton Trans.* **2015**, *44*, 11551−11561.
(28) Constable, E. C.; Thompson, A. M. W. C. A new ligand for the self assembly of starburst coordination oligomers and polymers. *J. Chem. Soc., Chem. Commun.* **1992**, 617−619.
(29) Masschelein, A.; Mesmaeker, A. K.-D.; Verhoeven, C.; Nasielski-Hinkens, R. Synthesis and characterization of a new non-linear trimetallic complex, hexakis(2,2′-bipyridine)-(μ-dipyrazino[2,3-

https://dx.doi.org/10.1021/acs.inorgchem.0c03004
Inorg. Chem. XXXX, XXX, XXX−XXX

f][2′,3′-h]quinoxaline)-trisruthenium(II) and related compounds. *Inorg. Chim. Acta* **1987**, *129*, L13−L16.
(30) Samy, N. A.; Alexander, V. New star-shaped trinuclear Ru(ii) polypyridine complexes of imidazo[4,5-f][1,10]phenanthroline derivatives: syntheses, characterization, photophysical and electrochemical properties. *Dalton Trans.* **2011**, *40*, 8630−8642.
(31) Ceroni, P.; Credi, A.; Balzani, V.; Campagna, S.; Hanan, G. S.; Arana, C. R.; Lehn, J.-M. Absorption and Emission Properties of Di- and Trinuclear Ruthenium(II) Rack-Type Complexes. *Eur. J. Inorg. Chem.* **1999**, *1999*, 1409−1414.
(32) Cheng, F.; Yu, S.; Ren, M.; He, C.; Yin, H. Di- and trinuclear Ru(II) complexes of 1,10-phenanthroline and 2,2′-bipyridine derivatives; synthesis, photophysical and electrochemical properties. *Transition Met. Chem.* **2016**, *41*, 305−314.
(33) Cheng, F.; He, C.; Yao, L.; Wang, F.; Tang, N. Three trinuclear Ru(II) complexes containing 4,5-diazafluorene and 2,2′-bipyridine: synthesis, absorption spectrum, luminescence, and redox behavior. *J. Coord. Chem.* **2015**, *68*, 704−716.
(34) Hasenknopf, B.; Hall, J.; Lehn, J. M.; Balzani, V.; Credi, A.; Campagna, S. Linear tris-terpyridines and their trinuclear Ru(II) complexes: synthesis, absorption spectra, and excited state properties. *New J. Chem.* **1996**, *20*, 725−730.
(35) Constable, E. C.; Handel, R. W.; Housecroft, C. E.; Farràn Morales, A.; Ventura, B.; Flamigni, L.; Barigelletti, F. Metal-Directed Synthesis and Photophysical Studies of Trinuclear V-Shaped and Pentanuclear X-Shaped Ruthenium and Osmium Metallorods and Metallostars Based upon 4′-(3,5-Dihydroxyphenyl)-2,2′:6′,2″-terpyridine Divergent Units. *Chem. - Eur. J.* **2005**, *11*, 4024−4034.
(36) Cerfontaine, S.; Marcélis, L.; Laramee-Milette, B.; Hanan, G. S.; Loiseau, F.; De Winter, J.; Gerbaux, P.; Elias, B. Converging Energy Transfer in Polynuclear Ru(II) Multiterpyridine Complexes: Significant Enhancement of Luminescent Properties. *Inorg. Chem.* **2018**, *57*, 2639−2653.
(37) Hanan, G. S.; Arana, C. R.; Lehn, J.-M.; Fenske, D. Synthesis, Structure, and Properties of Dinuclear and Trinuclear Rack-Type RuII Complexes. *Angew. Chem., Int. Ed. Engl.* **1995**, *34*, 1122−1124.
(38) Liu, D.; Jiang, Z.; Wang, M.; Yang, X.; Liu, H.; Wu, T.; Wang, P. Highly packed and stretched polyterpyridinyl Ru2+ complexes and their photophysical and stability properties. *Inorg. Chim. Acta* **2016**, *450*, 293−298.
(39) Connors, P. J.; Tzalis, D.; Dunnick, A. L.; Tor, Y. Coordination Compounds as Building Blocks: Single-Step Synthesis of Heteronuclear Multimetallic Complexes Containing RuII and OsII. *Inorg. Chem.* **1998**, *37*, 1121−1123.
(40) Luis, E. T.; Iranmanesh, H.; Arachchige, K. S. A.; Donald, W. A.; Quach, G.; Moore, E. G.; Beves, J. E. Luminescent Tetrahedral Molecular Cages Containing Ruthenium(II) Chromophores. *Inorg. Chem.* **2018**, *57*, 8476−8486.
(41) Harriman, A.; Khatyr, A.; Ziessel, R. The photophysical properties of short, linear arrays of ruthenium(II) tris(2,2′-bipyridine) complexes. *Res. Chem. Intermed.* **2007**, *33*, 49−62.
(42) Hilton, G. R.; Jackson, A. T.; Thalassinos, K.; Scrivens, J. H. Structural Analysis of Synthetic Polymer Mixtures Using Ion Mobility and Tandem Mass Spectrometry. *Anal. Chem.* **2008**, *80*, 9720−9725.
(43) Duez, Q.; Romain, M.; Tonneaux, C.; De Winter, J.; Lemaur, V.; Cornil, J.; Poriel, C.; Gerbaux, P. Discrimination of positional isomers by ion mobility mass spectrometry: application to organic semiconductors. *Anal. Methods* **2018**, *10*, 2303−2306.
(44) Troian-Gautier, L.; Marcélis, L.; De Winter, J.; Gerbaux, P.; Moucheron, C. Two ruthenium complexes capable of storing multiple electrons on a single ligand - photophysical, photochemical and electrochemical properties of [Ru(phen)2(TAPHAT)]2+ and [Ru(phen)2(TAPHAT)Ru(phen)2]4+. *Dalton Trans.* **2017**, *46*, 15287−15300.
(45) Troian-Gautier, L.; Moucheron, C. RutheniumII Complexes bearing Fused Polycyclic Ligands: From Fundamental Aspects to Potential Applications. *Molecules* **2014**, *19*, 5028−5087.
(46) Wang, Y.; Liu, S.; Pinto, M. R.; Dattelbaum, D. M.; Schoonover, J. R.; Schanze, K. S. Excited-State Structure and Delocalization in Ruthenium(II)-Bipyridine Complexes That Contain Phenyleneethynylene Substituents. *J. Phys. Chem. A* **2001**, *105*, 11118−11127.
(47) Zhu, S. S.; Kingsborough, R. P.; Swager, T. M. Conducting redox polymers: investigations of polythiophene-Ru(bpy)3 hybrid materials. *J. Mater. Chem.* **1999**, *9*, 2123−2131.
(48) Fuchs, Y.; Lofters, S.; Dieter, T.; Shi, W.; Morgan, R.; Strekas, T. C.; Gafney, H. D.; Baker, A. D. Spectroscopic and electrochemical properties of dimeric Ruthenium(II) diimine complexes and determination of their excited state redox properties. *J. Am. Chem. Soc.* **1987**, *109*, 2691−2697.
(49) Phifer, C. C.; McMillin, D. R. The basis of aryl substituent effects on charge-transfer absorption intensities. *Inorg. Chem.* **1986**, *25*, 1329−1333.
(50) Masschelein, A.; Jacquet, L.; Kirsch-De Mesmaeker, A.; Nasielski, J. Ruthenium complexes with 1,4,5,8-tetraazaphenanthrene. Unusual photophysical behavior of the tris-homoleptic compound. *Inorg. Chem.* **1990**, *29*, 855−860.
(51) Suzuki, K.; Kobayashi, A.; Kaneko, S.; Takehira, K.; Yoshihara, T.; Ishida, H.; Shiina, Y.; Oishi, S.; Tobita, S. Reevaluation of absolute luminescence quantum yields of standard solutions using a spectrometer with an integrating sphere and a back-thinned CCD detector. *Phys. Chem. Chem. Phys.* **2009**, *11*, 9850−9860.
(52) Ito, A.; Meyer, T. J. The Golden Rule. Application for fun and profit in electron transfer, energy transfer, and excited-state decay. *Phys. Chem. Chem. Phys.* **2012**, *14*, 13731−13745.
(53) Motley, T. C.; Troian-Gautier, L.; Brennaman, M. K.; Meyer, G. J. Excited-State Decay Pathways of Tris(bidentate) Cyclometalated Ruthenium(II) Compounds. *Inorg. Chem.* **2017**, *56*, 13579−13592.
(54) Caspar, J. V.; Westmoreland, T. D.; Allen, G. H.; Bradley, P. G.; Meyer, T. J.; Woodruff, W. H. Molecular and electronic structure in the metal-to-ligand charge-transfer excited states of d6 transition-metal complexes in solution. *J. Am. Chem. Soc.* **1984**, *106*, 3492−3500.
(55) Bradley, P. G.; Kress, N.; Hornberger, B. A.; Dallinger, R. F.; Woodruff, W. H. Vibrational spectroscopy of the electronically excited state. 5. Time-resolved resonance Raman study of tris(bipyridine)-ruthenium(II) and related complexes. Definitive evidence for the "localized" MLCT state. *J. Am. Chem. Soc.* **1981**, *103*, 7441−7446.
(56) Danzer, G. D.; Kincaid, J. R. Resonance Raman spectra of homoleptic and heteroleptic complexes of ruthenium(II) with bipyridine and bipyrazine in the ground and 3MLCT excited states. *J. Phys. Chem.* **1990**, *94*, 3976−3980.
(57) Caspar, J. V.; Sullivan, B. P.; Kober, E. M.; Meyer, T. J. Application of the energy gap law to the decay of charge transfer excited states, solvent effects. *Chem. Phys. Lett.* **1982**, *91*, 91−95.
(58) Kober, E. M.; Marshall, J. L.; Dressick, W. J.; Sullivan, B. P.; Caspar, J. V.; Meyer, T. J. Synthetic control of excited states. Nonchromophoric ligand variations in polypyridyl complexes of osmium(II). *Inorg. Chem.* **1985**, *24*, 2755−2763.
(59) Troian-Gautier, L.; Wehlin, S. A. M.; Meyer, G. J. Photophysical Properties of Tetracationic Ruthenium Complexes and Their Ter-Ionic Assemblies with Chloride. *Inorg. Chem.* **2018**, *57*, 12232−12244.
(60) Andersson, J.; Puntoriero, F.; Serroni, S.; Yartsev, A.; Pascher, T.; Polıvka, T.; Campagna, S.; Sundstrom, V. Ultrafast singlet energy transfer competes with intersystem crossing in a multi-center transition metal polypyridine complex. *Chem. Phys. Lett.* **2004**, *386*, 336−341.
(61) La Mazza, E.; Puntoriero, F.; Nastasi, F.; Laramee-Milette, B.; Hanan, G. S.; Campagna, S. A heptanuclear light-harvesting metal-based antenna dendrimer with six Ru(ii)-based chromophores directly powering a single Os(ii)-based energy trap. *Dalton Trans.* **2016**, *45*, 19238−19241.
(62) Wächtler, M.; Kübel, J.; Barthelmes, K.; Winter, A.; Schmiedel, A.; Pascher, T.; Lambert, C.; Schubert, U. S.; Dietzek, B. Energy transfer and formation of long-lived 3MLCT states in multimetallic complexes with extended highly conjugated bis-terpyridyl ligands. *Phys. Chem. Chem. Phys.* **2016**, *18*, 2350−2360.

https://dx.doi.org/10.1021/acs.inorgchem.0c03004
Inorg. Chem. XXXX, XXX, XXX−XXX

(63) Ohno, T.; Yoshimura, A.; Prasad, D. R.; Hoffman, M. Z. A weak.DELTA.G.degree. dependence of back electron transfer within the geminate redox pairs formed in the quenching of excited ruthenium(II) complexes by methyl viologen. *J. Phys. Chem.* **1991**, *95*, 4723−4728.
(64) McCusker, J. K. Femtosecond Absorption Spectroscopy of Transition Metal Charge-Transfer Complexes. *Acc. Chem. Res.* **2003**, *36*, 876−887.
(65) Amouyal, E.; Bahout, M.; Calzaferri, G. Excited states of M(II, d6)-4′-phenylterpyridine complexes: electron localization. *J. Phys. Chem.* **1991**, *95*, 7641−7649.
(66) Hager, G. D.; Crosby, G. A. Charge-transfer exited states of ruthenium(II) complexes. I. Quantum yield and decay measurements. *J. Am. Chem. Soc.* **1975**, *97*, 7031−7037.
(67) Hager, G. D.; Watts, R. J.; Crosby, G. A. Charge-transfer excited states of ruthenium(II) complexes. II. Relation of level parameters to molecular structure. *J. Am. Chem. Soc.* **1975**, *97*, 7037−7042.
(68) Lumpkin, R. S.; Kober, E. M.; Worl, L. A.; Murtaza, Z.; Meyer, T. J. Metal-to-ligand charge-transfer (MLCT) photochemistry: experimental evidence for the participation of a higher lying MLCT state in polypyridyl complexes of ruthenium(II) and osmium(II). *J. Phys. Chem.* **1990**, *94*, 239−243.
(69) Harriman, A.; Izzet, G. Direct observation of the fourth MLCT triplet state in ruthenium(ii) tris(2,2′-bipyridine). *Phys. Chem. Chem. Phys.* **2007**, *9*, 944−948.
(70) Allsopp, S. R.; Cox, A.; Kemp, T. J.; Reed, W. J. Inorganic photophysics in solution. Part 1.—Temperature activation of decay processes in the luminescence of tris(2,2′-bipyridine)ruthenium(II) and tris(1,10-phenanthroline)ruthenium(II) ions. *J. Chem. Soc., Faraday Trans. 1* **1978**, *74*, 1275−1289.
(71) Van Houten, J.; Watts, R. J. Temperature dependence of the photophysical and photochemical properties of the tris(2,2′-bipyridyl)ruthenium(II) ion in aqueous solution. *J. Am. Chem. Soc.* **1976**, *98*, 4853−4858.
(72) Forster, L. S. Thermal relaxation in excited electronic states of d3 and d6 metal complexes. *Coord. Chem. Rev.* **2002**, *227*, 59−92.
(73) Meyer, T. J. Photochemistry of metal coordination complexes: metal to ligand charge transfer excited states. *Pure Appl. Chem.* **1986**, *58*, 1193−1206.
(74) Abrahamsson, M.; Becker, H. C.; Hammarstrom, L. Micro-second 3MLCT excited state lifetimes in bis-tridentate Ru(ii)-complexes: significant reductions of non-radiative rate constants. *Dalton Trans* **2017**, *46*, 13314−13321.
(75) Barigelletti, F.; Juris, A.; Balzani, V.; Belser, P.; Von Zelewsky, A. Temperature dependence of the bis(2,2′-bipyridine)-dicyanoruthenium(II) and bis(2,2′-bipyridine)(2,2′-isobiquinoline)-ruthenium(II) luminescence. *J. Phys. Chem.* **1987**, *91*, 1095−1098.
(76) De Cola, L.; Barigelletti, F.; Cook, M. J. Photophysical Properties and Photochemical Behaviour of Ruthenium(II) complexes containing the 2,2′-bipyridine and 4,4′-diphenyl-2,2′-bipyridine ligands. *Helv. Chim. Acta* **1988**, *71*, 733−741.
(77) Allen, G. H.; White, R. P.; Rillema, D. P.; Meyer, T. J. Synthetic control of excited-state properties. Tris-chelate complexes containing the ligands 2,2′-bipyrazine, 2,2′-bipyridine, and 2,2′-bipyrimidine. *J. Am. Chem. Soc.* **1984**, *106*, 2613−2620.
(78) White, J. K.; Schmehl, R. H.; Turro, C. An overview of photosubstitution reactions of Ru(II) imine complexes and their application in photobiology and photodynamic therapy. *Inorg. Chim. Acta* **2017**, *454*, 7−20.
(79) Luis, E. T.; Iranmanesh, H.; Beves, J. E. Photosubstitution reactions in ruthenium(II) trisdiimine complexes: Implications for photoredox catalysis. *Polyhedron* **2019**, *160*, 1−9.
(80) Soupart, A.; Alary, F.; Heully, J.-L.; Elliott, P. I. P.; Dixon, I. M. Theoretical Study of the Full Photosolvolysis Mechanism of $[Ru(bpy)_3]^{2+}$: Providing a General Mechanistic Roadmap for the Photochemistry of $[Ru(N\text{-}N)3]^{2+}$-Type Complexes toward Both Cis and Trans Photoproducts. *Inorg. Chem.* **2020**, *59*, 14679−14695.
(81) Soupart, A.; Alary, F.; Heully, J.-L.; Elliott, P. I. P.; Dixon, I. M. Recent progress in ligand photorelease reaction mechanisms: Theoretical insights focusing on Ru(II) 3MC states. *Coord. Chem. Rev.* **2020**, *408*, 213184.
(82) Soupart, A.; Alary, F.; Heully, J.-L.; Elliott, P. I. P.; Dixon, I. M. Exploration of Uncharted 3PES Territory for [Ru(bpy)3]2+: A New 3MC Minimum Prone to Ligand Loss Photochemistry. *Inorg. Chem.* **2018**, *57*, 3192−3196.
(83) Durham, B.; Caspar, J. V.; Nagle, J. K.; Meyer, T. J. Photochemistry of tris(2,2′-bipyridine)ruthenium(2+) ion. *J. Am. Chem. Soc.* **1982**, *104*, 4803−4810.
(84) Caspar, J. V.; Meyer, T. J. Photochemistry of MLCT excited states. Effect of nonchromophoric ligand variations on photophysical properties in the series cis-Ru(bpy)2L22+. *Inorg. Chem.* **1983**, *22*, 2444−2453.
(85) Yersin, H.; Rausch, A. F.; Czerwieniec, R.; Hofbeck, T.; Fischer, T. The triplet state of organo-transition metal compounds. Triplet harvesting and singlet harvesting for efficient OLEDs. *Coord. Chem. Rev.* **2011**, *255*, 2622−2652.
(86) Wilson, J. S.; Chawdhury, N.; Al-Mandhary, M. R. A.; Younus, M.; Khan, M. S.; Raithby, P. R.; Köhler, A.; Friend, R. H. The Energy Gap Law for Triplet States in Pt-Containing Conjugated Polymers and Monomers. *J. Am. Chem. Soc.* **2001**, *123*, 9412−9417.
(87) Baiano, J. A.; Murphy, W. R. Nonradiative decay in rhenium(I) monometallic complexes of 2,3-di-2-pyridylpyrazine. *Inorg. Chem.* **1991**, *30*, 4594−4598.
(88) Damrauer, N. H.; McCusker, J. K. Variable-Temperature Emission Studies of Solvation Dynamics: Evidence for Coupling of Solvation to Chromophore Structural Dynamics in the Evolution of Charge-Transfer Excited States. *Inorg. Chem.* **1999**, *38*, 4268−4277.
(89) Barigelletti, F.; Juris, A.; Balzani, V.; Belser, P.; Von Zelewsky, A. Temperature dependence of the luminescence emission of ruthenium(II) complexes containing the ligands 2,2′-bipyridine and dipyrido[3,2-c:2′,3′-e]pyridazine. *J. Phys. Chem.* **1986**, *90*, 5190−5193.
(90) Barigelletti, F.; Juris, A.; Balzani, V.; Belser, P.; Von Zelewsky, A. Excited-state properties of complexes of the tris(diimine)-ruthenium(2+) ion family. *Inorg. Chem.* **1983**, *22*, 3335−3339.
(91) Benniston, A. C.; Harriman, A.; Li, P.; Sams, C. A. Comparison of the Photophysical Properties of Osmium(II) Bis(2,2′:6′,2″-terpyridine) and the Corresponding Ethynylated Derivative. *J. Phys. Chem. A* **2005**, *109*, 2302−2309.
(92) Harriman, A.; Izzet, G.; Goeb, S.; Nicola, A. D.; Ziessel, R. Photophysical Properties of Ruthenium(II) Tris(2,2′-bipyridine) Complexes Bearing Conjugated Thiophene Appendages. *Inorg. Chem.* **2006**, *45*, 9729−9741.
(93) Barigelletti, F.; Belser, P.; Von Zelewsky, A.; Juris, A.; Balzani, V. Luminescence of mixed-ligand polypyridine-ruthenium(II) complexes in the temperature range 84−250 K. Interligand interactions and viscosity effects on radiationless processes. *J. Phys. Chem.* **1985**, *89*, 3680−3684.

https://dx.doi.org/10.1021/acs.inorgchem.0c03004
Inorg. Chem. XXXX, XXX, XXX−XXX